LUND UNIVERSITY

LTH

FACULTY OF ENGINEERING

Emissive State Dynamics of Quasi-2D Lead Halide Perovskite Single Crystals

Chenyang Gu

A thesis submitted for the degree of Master's in Photonics

Department of Chemistry
Division of Chemical Physics
Lund University

Supervisor: Kaibo Zheng

Examiner: Cord Arnold

Abstract

Quasi-two-dimensional (quasi-2D) metal halide perovskites (MHPs) are important low-dimensional semiconductor systems because of their strong excitonic response, tunable emission properties, and improved structural stability compared with conventional three-dimensional (3D) perovskites. In these materials, the inorganic layer thickness and the molecular structure of the organic spacer can modulate quantum confinement, exciton localization, and excited-state relaxation pathways. Understanding these structure-dependent photophysical processes is therefore important for the rational design of perovskite-based optoelectronic materials.

This thesis investigates the emissive-state dynamics of quasi-2D lead halide perovskite single crystals, various quantum well thickness n-pentylammonium lead bromide (n-PAPB) ($n = 1$), n-PAPB ($n = 2$), as well as the organic spacer n-PAPB ($n = 2$), n-butylammonium methylammonium lead bromide (n-BAPB) ($n = 2$), and iso-butylammonium methylammonium lead bromide (iso-BAPB) ($n = 2$)). Steady-state absorption spectroscopy, photoluminescence (PL) spectroscopy, temperature-dependent PL spectroscopy, time-resolved photoluminescence (TRPL), and transient absorption (TA) spectroscopy were used to examine their optical properties and excited-state dynamics.

The absorption and PL spectra suggest the coexistence of multiple quasi-2D domains, likely dominated by $n = 1 - 3$ phases. Excitation intensity-dependent PL measurements show nearly linear intensity scaling with excitation power, which can be attributed to the dominated excitonic radiative recombination under the investigated excitation conditions. Temperature-dependent PL measurements reveal pronounced electron-phonon interactions that influence the charge carrier recombination at the emissive states. The extracted exciton binding energies are approximately 84-110 meV, indicating strongly localized excitonic states in these quasi-2D structures. Linewidth broadening analysis further suggests coupling between excitons and longitudinal optical phonons. TA spectroscopy indicates ultrafast charge carrier relaxation followed by the formation of long-lived localized excited states.

Overall, this work shows that both inorganic layer thickness and spacer molecular structure are closely correlated with the excited-state dynamics of quasi-2D perovskites. The

results provide insight into structure-dependent exciton localization, carrier-phonon interactions, and emissive-state relaxation processes in layered perovskite systems.

Keywords: quasi-2D perovskites; lead halide perovskites; photoluminescence; transient absorption; electron-phonon coupling.

Acknowledgements

I would like to express my sincere gratitude to everyone who has supported me throughout my Master's study and during the completion of this thesis. This work would not have been possible without the guidance, encouragement, and help I received from many people around me.

First of all, I would like to express my deepest thanks to my supervisor, Prof. Kaibo Zheng, for his patient guidance, continuous support, and valuable advice throughout this project. His rigorous attitude towards research, thoughtful suggestions, and constant encouragement have greatly shaped my academic growth and helped me complete this thesis successfully.

I also sincerely thank Prof. Tönu Pullerits for generously providing access to the experimental facilities and research environment that made this work possible. His support is greatly appreciated.

Special thanks go to Dr. Mingli Liang, Dr. Zehan Yao, Dr. Yanmei He, Dr. Qinying Pan, and Dr. Ahmed Magdy Kobaisy for their kind help, insightful discussions, and support during my research and experiments. Their experience, patience, and suggestions were extremely valuable during this project.

I am also grateful to all my classmates and friends in the Photonics programme. Studying with such talented and passionate people made this journey both enjoyable and inspiring. Meanwhile, I would like to thank my friends from other programs and my undergraduate alumni friends for their companionship and support during my time in Sweden.

My sincere appreciation also goes to Prof. Cord Arnold, Program Director of the Photonics programme, for his help and support regarding academic and study-related matters during my studies. I also would like to thank International Coordinator Helene von Wachenfelt for her kindness and assistance in many aspects of daily life, which helped me adapt more smoothly to life in Lund.

Special thanks are also given to the friends who came to Sweden to visit me. Your companionship and the memorable moments we shared brought me great happiness and

warmth during my time abroad.

Furthermore, I would like to express my gratitude to Lund University and the city of Lund itself for providing such a unique academic environment, where long-standing traditions coexist with innovation and openness. The experience of studying and living in Lund has left me with memories and friendships that I will always cherish.

Last but not least, I would like to thank my parents and family for their unconditional love, understanding, and continuous support. Their encouragement has always been my greatest motivation throughout this journey.

Popular Science Summary

Efficient light-emitting and light-absorbing materials are essential for modern optoelectronic technologies, including solar cells, LEDs, lasers, and photodetectors. Metal halide perovskites have attracted broad interest because their optical properties can be tuned by changing their chemical composition and crystal structure.

This thesis focuses on quasi-two-dimensional (quasi-2D) perovskites. In these materials, thin inorganic layers are separated by organic molecules, forming structures that resemble natural quantum wells. This layered arrangement confines electrons and holes within the inorganic regions and gives rise to strong light-emission properties.

The aim of this work was to understand how the thickness of the inorganic layers and the structure of the organic molecules affect light emission in quasi-2D perovskite single crystals. Several crystals were studied using optical spectroscopy methods, including steady-state and time-resolved measurements. These techniques make it possible to follow how excited carriers and excitons relax after light absorption.

The results show that the investigated crystals exhibit strong excitonic emission and clear interactions between excited carriers and lattice vibrations. The emission behavior depends on both the inorganic layer thickness and the organic spacer structure. In particular, the branched organic spacer leads to broader and red-shifted emission, suggesting stronger lattice distortion and enhanced exciton localization.

Ultrafast transient absorption measurements further show that photoexcited carriers relax rapidly after excitation and can form long-lived localized excited states. These processes are closely related to carrier-phonon interactions and local structural distortion in the quasi-2D lattice.

Overall, this thesis improves the understanding of how structural factors control light-emission processes in quasi-2D perovskites. Such knowledge may help guide the design of perovskite materials with improved emission properties and stability.

Contents

Acronyms

3D Three-dimensional

AC Alternating Cation

APD Avalanche Photodiode

DJ Dion–Jacobson

EQE External Quantum Efficiency

ESA Excited-state Absorption

FWHM Full Width at Half Maximum

GSB Ground-state Bleaching

LED Light-emitting Diode

MHP Metal Halide Perovskite

n-BAPB n-butylammonium Methylammonium Lead Bromide

n-PAPB n-pentylammonium Lead Bromide

PL Photoluminescence

quasi-2D Quasi-two-dimensional

RP Ruddlesden–Popper

STE Self-trapped Exciton

SVD Singular Value Decomposition

TA Transient Absorption

TCSPC Time-Correlated Single Photon Counting

TRPL Time-resolved Photoluminescence

iso-BAPB iso-butylammonium Methylammonium Lead Bromide

List of Figures

List of Tables

Chapter 1

Introduction

This chapter introduces the structural and basic photophysical properties of perovskite materials, with emphasis on quasi-2D MHPs. The roles of inorganic layer thickness and organic spacer cations are discussed in relation to quantum confinement, exciton localization, and excited-state dynamics. Representative optoelectronic applications, particularly solar cells and light-emitting diodes (LEDs), are then briefly reviewed. Finally, the motivation and objectives of this thesis are presented.

1.1 Perovskite Materials

Perovskite materials were first discovered in 1839 by Gustav Rose in calcium titanate ($CaTiO_3$) minerals found in the Ural Mountains of Russia and were later named after the Russian mineralogist Lev Perovski [1]. Since then, perovskites have evolved into a versatile class of functional materials with versatile crystal structures and diverse physical properties. The perovskite structure is commonly described by the general chemical formula ABX_3, where A and B represent cations of different ionic sizes and X denotes an anion, typically oxygen or a halide [2]. Early studies mainly focused on oxide perovskites such as $BaTiO_3$, which exhibited outstanding ferroelectric and piezoelectric properties and enabled applications in electronic and memory devices [3].

In recent decades, MHPs are now among the most widely studied solution-processable semiconductors. Inorganic perovskites such as $CsPbX_3$ ($X = Cl, Br, and\ I$) were initially synthesized in the late nineteenth century [4], while hybrid organic–inorganic perovskites including $MAPbX_3$ and $FAPbX_3$ were later developed and extensively investigated for their exceptional optoelectronic properties [5, 6]. Owing to their strong optical absorption [7–9], tunable bandgaps [10,11], and excellent emission characteristics [12,13], MHPs have attracted significant attention for applications in solar cells, LEDs, lasers, and photodetectors.

The optical and electronic properties of MHPs can be tuned through compositional engineering [14, 15], dimensional control [16, 17], and halide substitution [18, 19]. Their solution-processable nature also enables low-temperature fabrication and integration into different device architectures [20]. Beyond these practical advantages, quasi-2D MHPs exhibit rich photophysical behavior, including pronounced excitonic effects [21]. This is particularly relevant for low-dimensional perovskites, where structural confinement can substantially modify exciton formation, carrier relaxation, and light-emission processes.

1.2 Quasi-2D Perovskites

MHPs have attracted extensive interest for optoelectronic applications because of their excellent optical and electronic properties. However, despite the high performance achieved in conventional three-dimensional (3D) perovskites, insufficient environmental stability remains a major challenge for practical device applications [22, 23]. Exposure to moisture, oxygen, heat, and continuous illumination can induce structural degradation and deteriorate device performance. To improve material stability, quasi-2D perovskites have been developed by incorporating bulky organic spacer cations into the perovskite framework. Because these organic spacer molecules are generally hydrophobic, they can effectively suppress moisture penetration and enhance the environmental stability of the materials compared with conventional 3D perovskites [24]. As a result, quasi-2D perovskites have become important low-dimensional systems for stable optoelectronic applications.

3D MHPs possess a continuous network of corner-sharing BX_6 octahedra, forming the typical ABX_3 crystal structure (Fig. 1.1 a). By incorporating bulky organic ammonium spacer cations into the 3D framework, the continuous inorganic network can be periodically separated into layered structures [25]. This structural modification leads to the formation of low-dimensional perovskites. Depending on the arrangement and connectivity of the organic spacer layers, several types of layered perovskite structures can be obtained, including the Ruddlesden–Popper (RP), Dion–Jacobson (DJ), and alternating cation (AC) phases (Fig. 1.1 b).

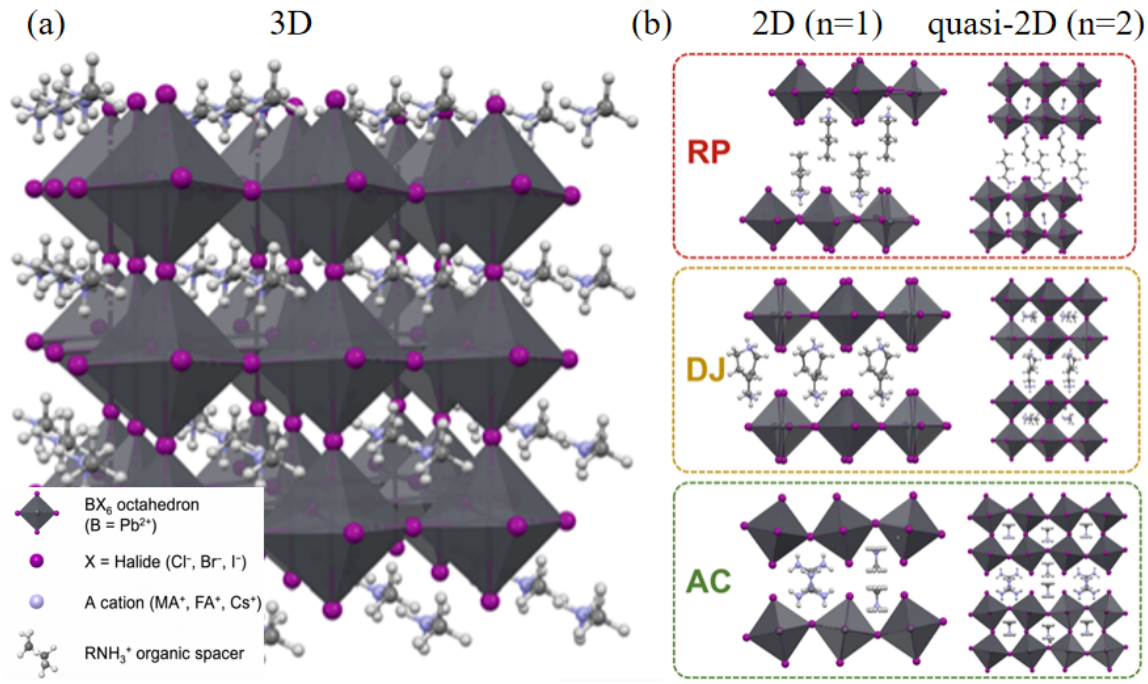

Figure 1.1: Schematic diagram of halide perovskite materials: (a) 3D halide perovskite materials. (b) 2D and quasi-2D halide perovskite materials. Figures were taken from Reference [25] with permission.

Compared with conventional 3D perovskites, these layered structures exhibit stronger confinement effects and greater structural flexibility. These characteristics strongly influence their optical and photophysical properties. Among them, RP-phase perovskites have received particular attention because of their pronounced excitonic characteristics and highly tunable photophysical behavior [26].

The general chemical formula of RP perovskites can be expressed as

$$(RNH_3)_2A_{n-1}B_nX_{3n+1} \tag{1.1}$$

where RNH_3^+ represents a bulky organic ammonium spacer cation, A denotes a small monovalent cation such as methylammonium (MA), formamidinium (FA), or cesium (Cs), B is typically Pb^{2+}, and X corresponds to a halide anion. In RP structures, inorganic metal-halide octahedral layers are periodically separated by organic spacer layers, forming natural quantum-well structures [27]. The dielectric constant of the organic spacer layer is significantly lower than that of the inorganic framework. This dielectric mismatch enhances the Coulomb interaction between electrons and holes and consequently strengthens excitonic effects in quasi-2D perovskites.

Another important parameter in RP perovskites is the inorganic layer thickness, which is commonly represented by the n value. The n value corresponds to the number of

connected inorganic octahedral layers confined between adjacent organic spacer layers. When $n = 1$, the structure contains only a single inorganic octahedral layer and exhibits the strongest two-dimensional characteristics. As the n value increases, the thickness of the inorganic slab gradually increases and the material properties progressively approach those of bulk 3D perovskites.

Reduced dimensionality in quasi-2D perovskites gives rise to pronounced quantum and dielectric confinement effects. Charge carriers are spatially confined within the inorganic layers, resulting in quantized electronic states and enhanced excitonic behavior. As a result, quasi-2D perovskites usually exhibit larger exciton binding energies than conventional 3D perovskites. These materials typically exhibit intense excitonic emission and high photoluminescence quantum yields.

Besides inorganic layer thickness, the molecular structure of the organic spacer cation also plays a critical role in determining the structural and optical properties of quasi-2D perovskites. Variations in spacer length, molecular arrangement, and steric effects may influence octahedral distortion, interlayer coupling, and quantum confinement [28, 29]. These structural variations may further influence exciton localization, emission characteristics, and excited-state dynamics. Therefore, organic spacer engineering has become an effective strategy for tuning the photophysical properties of quasi-2D perovskites.

1.3 Inorganic Layer Thickness and Organic Spacer Effects

The optical and photophysical properties of quasi-2D perovskites are closely linked to the inorganic layer thickness and the organic spacer cations.

The inorganic layer thickness determines the degree of quantum and dielectric confinement. In general, smaller n values lead to stronger confinement and larger exciton binding energies, whereas increasing n gradually shifts the material properties toward those of bulk 3D perovskites [30]. As a result, variations in n can modify the emission energy, charge carrier recombination dynamics, and carrier transport behavior.

The organic spacer cation provides an additional structural degree of freedom. Different spacer molecules can change the interlayer distance, octahedral distortion, molecular packing, and local dielectric environment [31, 32]. These structural changes can affect exciton localization, electron-phonon interactions, and emission linewidth. In particular, linear and branched spacer cations may lead to different lattice distortions and local structural disorder.

Therefore, comparing quasi-2D perovskites with different n values and spacer cations

provides a useful route to understand how structural factors control excited-state dynamics. In this work, single crystals were selected because their reduced defect densities and absence of grain boundaries enable more reliable investigation of intrinsic optical and excited-state properties compared with polycrystalline thin films [33]. The investigated systems included n-PAPB ($n = 1$), n-PAPB ($n = 2$), iso-BAPB ($n = 2$), and n-BAPB ($n = 2$), which were selected as representative quasi-2D perovskite systems with different inorganic layer thicknesses and spacer molecular structures.

1.4 Optoelectronic Applications

MHPs have been widely investigated for optoelectronic applications because of their strong optical absorption, tunable bandgaps, and efficient radiative recombination properties. Their favorable photophysical characteristics make them promising materials for photovoltaic devices, LEDs, lasers, and photodetectors.

1.4.1 Solar Cells

Photovoltaic devices convert sunlight into electricity and are a major platform for renewable energy technologies. In this context, MHPs have been widely investigated as light absorbers because of their strong optical absorption, tunable bandgaps, and long carrier diffusion lengths [34].

MHPs have emerged as promising photovoltaic materials because of their excellent optical and electronic properties [35]. These materials exhibit high absorption coefficients over a broad spectral range, long carrier diffusion lengths, and tunable bandgaps, making them promising candidates for high-performance solar cells. Since the first report of perovskite-based solar cells in 2009, the certified power conversion efficiencies of perovskite-based photovoltaic devices have increased rapidly from below 4 % to values exceeding 30 % [36–38], highlighting the remarkable potential of perovskite photovoltaic technologies. Several representative architectures of perovskite solar cells are illustrated in Fig. 1.2.

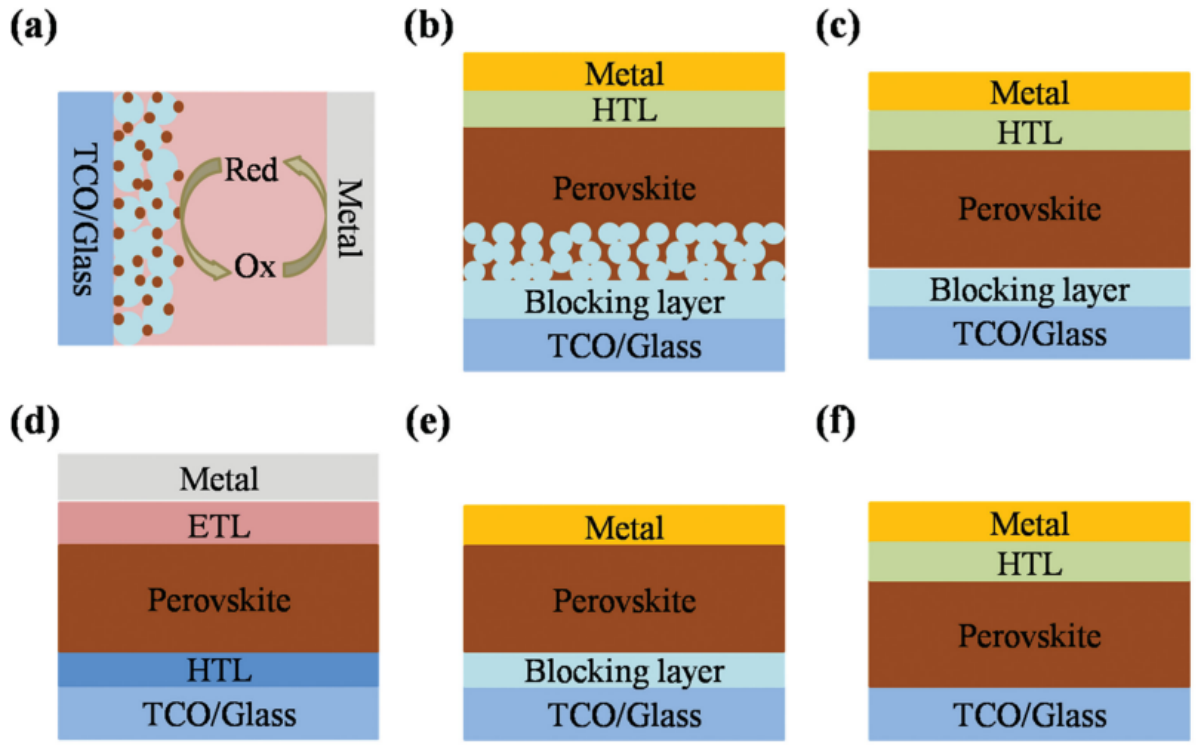

Figure 1.2: Typical structures for perovskite solar cells. TCO: transparent conducting oxide, HTL: hole transport layer, ETL: electron transport layer. Figures were taken from Reference [39] with permission.

Compared with conventional silicon solar cells, perovskite solar cells can be fabricated through low-temperature solution-processing methods, thereby significantly reducing fabrication cost and processing complexity [40]. In addition, the bandgap of perovskite materials can be readily tuned through compositional engineering and dimensional modulation, enabling flexible optimization of light absorption and carrier transport properties.

Although conventional 3D perovskites exhibit excellent photovoltaic performance, their practical applications are still limited by insufficient environmental stability. Quasi-2D perovskites have attracted increasing attention because the introduction of bulky organic spacer cations can improve moisture resistance and structural stability. In particular, layered perovskites exhibit enhanced resistance against heat and humidity compared with their 3D counterparts [41]. However, reduced dimensionality and strong quantum confinement may also influence charge transport behavior [42]. Clarifying the relationship between crystal structure and excited-state dynamics is necessary for further improving the photovoltaic performance of quasi-2D perovskites.

1.4.2 Light-emitting Diodes

LEDs are widely used in display technologies, solid-state lighting, and optical communication systems. High-performance light-emitting materials are generally required to

possess high emission efficiency, narrow emission linewidths, and tunable emission wavelengths [43]. MHPs have attracted considerable attention for LED applications because of their excellent luminescence properties and facile spectral tunability [44].

Perovskite LEDs have developed rapidly in recent years. Owing to their high photoluminescence quantum yields, narrow emission bandwidths, and solution-processable fabrication methods, perovskite materials have emerged as promising materials for next-generation light-emitting devices. Since the first demonstration of perovskite LEDs in 2014, the device performance has improved substantially [43]. The performance of LEDs is commonly evaluated using the external quantum efficiency (EQE), which describes the ratio between the number of emitted photons and injected charge carriers. In recent years, the EQEs of state-of-the-art perovskite LEDs have exceeded 30%, demonstrating their strong potential for high-performance light-emission applications [45]. The emission wavelength of perovskites can be effectively tuned across the visible spectral range through halide composition engineering and dimensional modulation [46]. Fig. 1.3 shows the emission wavelengths of different perovskite LEDs.

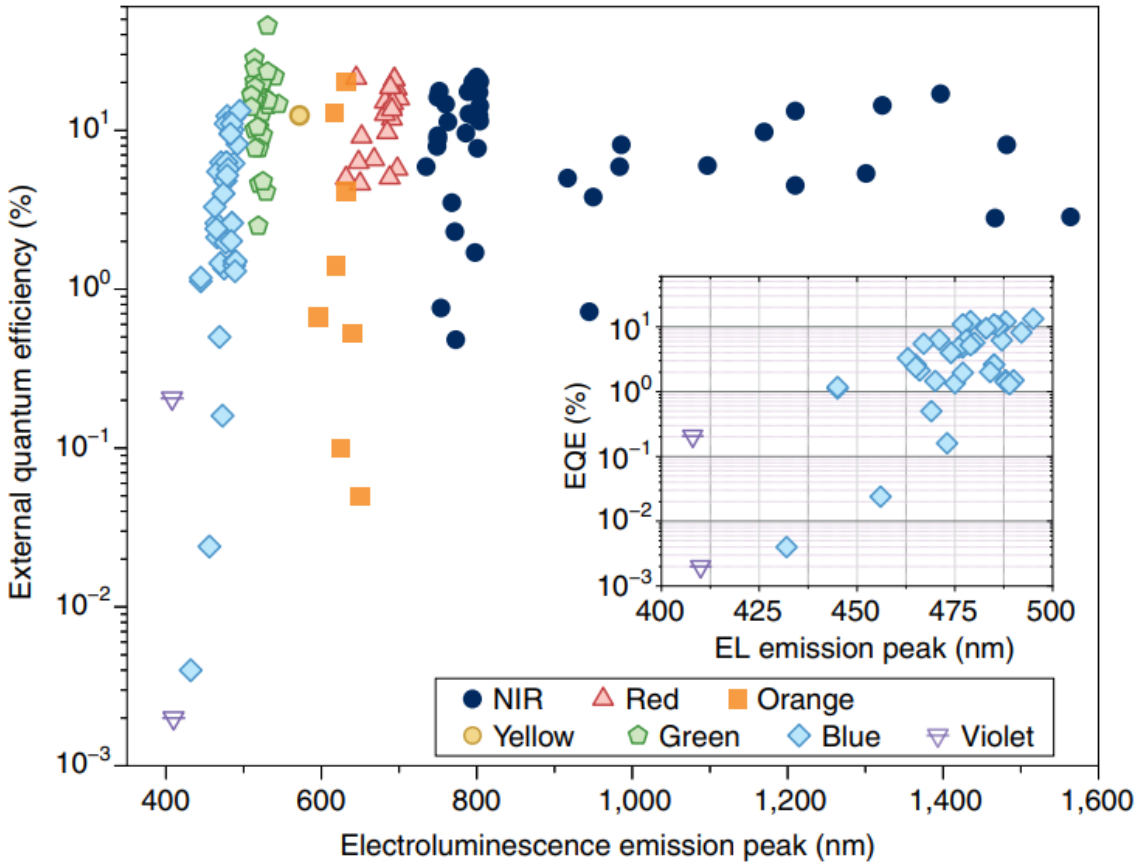

Figure 1.3: Electroluminescence of different perovskite LEDs. This figure was taken from Reference [47] with permission.

Quasi-2D perovskites are particularly attractive for LED applications because strong

quantum confinement can enhance radiative recombination efficiency. Compared with conventional 3D perovskites, layered structures usually exhibit larger exciton binding energies and reduced nonradiative recombination. These characteristics are favorable for efficient light emission. For example, quasi-2D perovskites have demonstrated highly efficient electroluminescence in perovskite LED devices [48].

The emission properties of quasi-2D perovskites are closely related to their crystal structures and excited-state dynamics. Variations in inorganic layer thickness and organic spacer cations may influence exciton localization, electron-phonon interactions, and carrier relaxation processes. In addition, strong electron-phonon coupling and flexible lattice structures in low-dimensional perovskites can promote the formation of self-trapped excitons (STEs), which may lead to broadband white-light emission [49]. Therefore, investigating the photophysical behavior of quasi-2D perovskites is important for understanding their emission mechanisms and optimizing the performance of perovskite-based LEDs.

1.5 Motivation and Objectives

The optical and photophysical properties of quasi-2D perovskites are governed by a combination of inorganic layer thickness, organic spacer structure, and local lattice distortion. Although these materials often show strong excitonic emission and improved stability compared with conventional 3D perovskites, the relationship between structural variation and excited-state relaxation remains incompletely understood. In particular, the effects of spacer geometry and dimensionality on carrier relaxation, exciton localization, and emissive-state formation require further investigation.

In this thesis, quasi-2D perovskite single crystals with different inorganic layer thicknesses and organic spacer cations were studied, including n-PAPB ($n = 1$), n-PAPB ($n = 2$), iso-BAPB ($n = 2$), and n-BAPB ($n = 2$). Their optical responses and excited-state dynamics were investigated using absorption spectroscopy, PL spectroscopy, temperature-dependent PL, TRPL, and TA spectroscopy. By comparing these systems, this work aims to clarify how dimensionality and spacer molecular structure affect excitonic emission, carrier-phonon coupling, and excited-state relaxation in quasi-2D perovskites.

Chapter 2

Theoretical Background

This chapter introduces the theoretical background relevant to the optical and photophysical properties of quasi-2D perovskites investigated in this thesis. The fundamental concepts related to excitonic behavior, carrier recombination, and electron-phonon interactions are briefly discussed. Meanwhile, the principles of PL, TRPL, and TA spectroscopy are introduced to provide the theoretical basis for the experimental investigations presented in the following chapters.

2.1 Excitons and Quantum Confinement in Quasi-2D Perovskites

In semiconductors, optical excitation with photon energies larger than the bandgap energy (E_g) can generate electron-hole pairs. Because of the Coulomb attraction between electrons and holes, bound quasiparticles known as excitons may be formed [50]. Excitons are generally classified into Frenkel excitons and Wannier-Mott excitons according to the spatial distribution of the electron-hole pair. Frenkel excitons are strongly localized within a single unit cell, whereas Wannier-Mott excitons possess much larger radii and are weakly bound in the crystal lattice. Excitons in MHPs generally belong to the Wannier-Mott type [51].

The excitonic energy levels can be approximated using a hydrogen-like model [51]:

$$E_n = E_g - \frac{E_b}{n^2} \tag{2.1}$$

where E_g is the bandgap energy, E_b is the exciton binding energy, and n is the principal quantum number. The exciton binding energy corresponds to the energy required for dissociating excitons into free charge carriers. Reduced dimensionality and dielectric

confinement in quasi-2D perovskites generally result in larger E_b values than those in conventional 3D perovskites [52].

Experimentally, the exciton binding energy can be estimated through several spectroscopic approaches, including absorption spectroscopy, temperature-dependent PL, and ultrafast spectroscopic techniques [53, 54]. Temperature-dependent PL measurements were used to estimate the exciton binding energy associated with thermal activation processes. In the ideal case where trap states are neglected, the integrated PL intensity as a function of temperature can be fitted using the Arrhenius equation [28, 55, 56]:

$$I(T) = \frac{I_0}{1 + Ae^{-E_b/k_B T}} \tag{2.2}$$

where I_0 is the PL intensity at low temperature, A is a fitting constant and k_B is the Boltzmann constant ($k_B = 8.617 \times 10^{-5}$ eV K^{-1}). Since quasi-2D perovskites generally exhibit strong excitonic emission, the excited-state dynamics in these materials are mainly dominated by excitonic recombination processes.

Variations in inorganic layer thickness and spacer molecular structure can lead to different degrees of quantum confinement in quasi-2D perovskites, which further influence the exciton binding energy (E_b). Smaller n values generally result in stronger confinement effects and larger E_b values, while increasing the inorganic layer thickness gradually leads to weaker confinement and more bulk-like behavior. Notably, different organic spacer cations may influence lattice distortion and dielectric environments, which can further affect exciton localization and excitonic recombination processes. Therefore, the photophysical properties of n-PAPB ($n = 1$), n-PAPB ($n = 2$), iso-BAPB ($n = 2$), and n-BAPB ($n = 2$) are expected to exhibit different excitonic characteristics and excited-state dynamics.

Fig. 2.1 illustrates the crystal structures and corresponding confinement potentials of bulk and quasi-2D perovskites with different inorganic layer thicknesses and organic spacer cations. As the dimensionality decreases from bulk 3D perovskites to quasi-2D structures, stronger quantum confinement can enhance the Coulomb interaction between electrons and holes, resulting in larger exciton binding energies [41, 52]. Moreover, variations in spacer molecular structure may further modify the dielectric environment and confinement potential, leading to different excitonic properties among n-PAPB ($n = 1$), n-PAPB ($n = 2$), iso-BAPB ($n = 2$), and n-BAPB ($n = 2$).

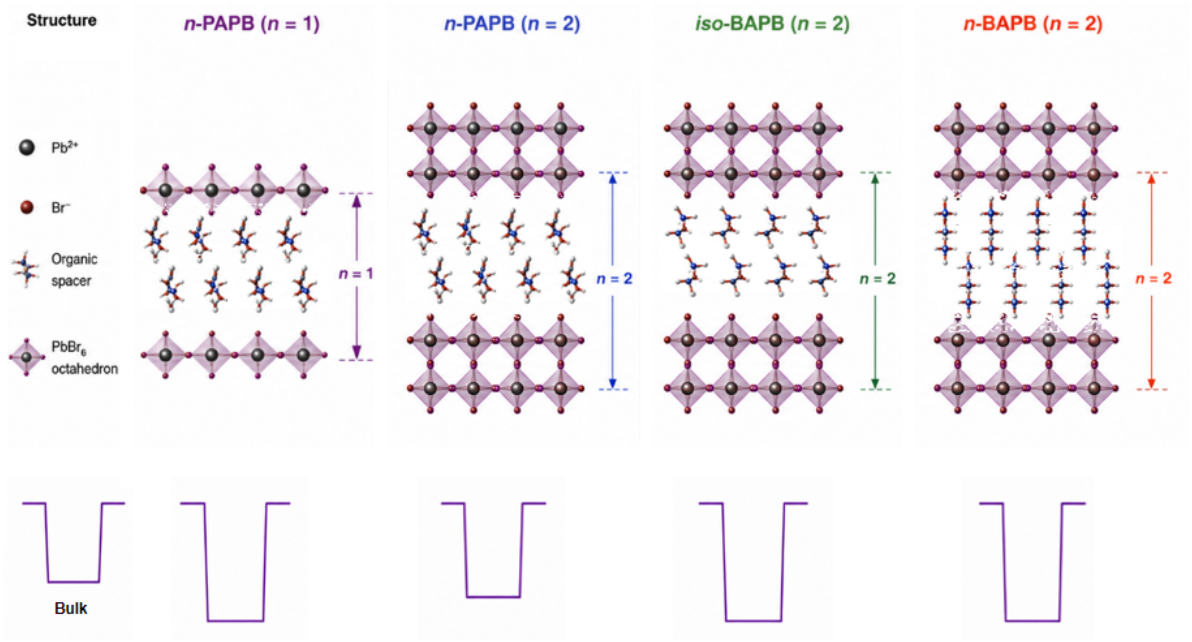

Figure 2.1: Crystal structures and confinement potentials of quasi-2D perovskites.

2.2 Excited-state Dynamics

After optical excitation with photon energies exceeding the bandgap, electrons in the valence band can be excited to the conduction band, leaving holes in the valence band. In quasi-2D perovskites, the Coulomb interaction between electrons and holes can lead to the formation of excitons because of the strong quantum confinement and relatively large exciton binding energies [41].

After photoexcitation, the excited carriers may undergo several relaxation pathways back to the ground states, including radiative and nonradiative recombination. In radiative recombination processes, electrons recombine radiatively with holes, producing photoluminescence emission. In contrast, nonradiative recombination processes dissipate excitation energy to the lattice through phonon emission via defect- or trap-mediated relaxation pathways rather than photon emission [57]. Defect states and lattice imperfections can act as carrier trapping centers, thereby modifying the carrier relaxation pathways and excited-state lifetimes. The corresponding radiative recombination pathways, including band-to-band luminescence, excitonic luminescence, and STE luminescence, are schematically illustrated in Fig. 2.2.

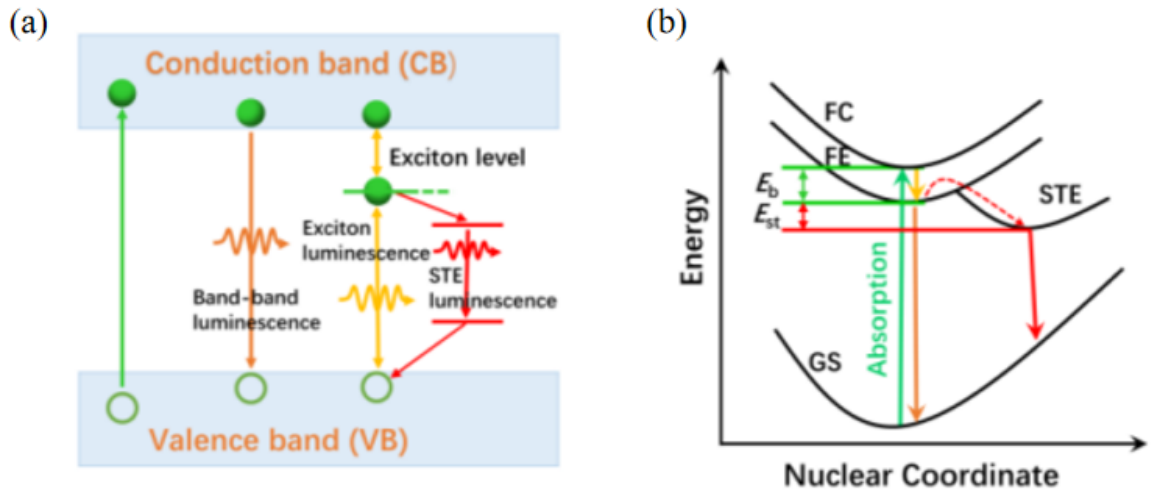

Figure 2.2: (a) Schematic illustration of intrinsic photoluminescence processes in perovskite materials, including band-to-band luminescence, excitonic luminescence, and STE luminescence. (b) Schematic illustration of the energy level structure associated with STE formation and relaxation processes (GS, ground state; FE, free exciton state; FC, free carrier state; E_b, exciton binding energy; E_{st}, self-trapping energy). This figure was taken from Reference [58] with permission.

In addition to free excitonic recombination, STEs may also form in low-dimensional perovskite materials because of strong electron-phonon coupling and flexible lattice structures [59, 60]. Under strong lattice interactions, the excited carriers can induce local lattice distortion and become localized in a lower-energy self-trapped state. Compared with free-exciton emission, STE emission usually exhibits broader and more red-shifted luminescence bands. In quasi-2D perovskites, reduced dimensionality and lattice softness can favor STE formation and influence the excited-state relaxation dynamics.

In quasi-2D perovskites, the reduced dimensionality and strong confinement effects can enhance excitonic recombination processes. Moreover, variations in inorganic layer thickness and spacer molecular structure may influence carrier localization and recombination dynamics. Octahedral distortion and local dielectric screening can additionally modify carrier relaxation pathways and emission behavior.

Excited-state recombination behavior can be evaluated using excitation power-dependent PL measurements. The relationship between PL intensity and excitation power is commonly described by

$$I_{PL} \propto P^k \tag{2.3}$$

where I_{PL} is the integrated PL intensity, P is the excitation power, and k is the power-law coefficient. A k value close to 1 generally indicates monomolecular recombination behavior

and a nearly linear relationship between PL intensity and excitation power. In quasi-2D perovskites, this behavior is commonly attributed to excitonic radiative recombination [56, 61]. A k value approaching 2 is typically associated with bimolecular free-carrier recombination, whereas values smaller than 1 may indicate trap-assisted nonradiative recombination or saturation effects. Intermediate k values may suggest the coexistence of multiple recombination pathways. Therefore, the power-law coefficient can provide useful insight into the dominant excited-state relaxation and recombination mechanisms in quasi-2D perovskites.

Because of the different confinement strengths and dielectric environments in n-PAPB ($n = 1$), n-PAPB ($n = 2$), iso-BAPB ($n = 2$), and n-BAPB ($n = 2$), distinct excited-state relaxation and recombination dynamics are anticipated in these quasi-2D perovskite systems.

2.3 Electron-phonon Coupling

Electron-phonon interactions are critical for understanding excited-state dynamics in perovskite materials. Interactions between charge carriers and lattice vibrations (phonons) can significantly affect relaxation dynamics, carrier mobility, and radiative recombination behavior [62, 63]. In low-dimensional perovskites, the soft lattice structure and reduced dimensionality can further enhance electron-phonon interactions. Strong electron–phonon coupling means that excited carriers interact strongly with lattice vibrations, which can locally distort the crystal lattice, localize excitons, and promote the formation of STEs, a phenomenon commonly observed in quasi-2D perovskite systems [64].

Temperature-dependent PL linewidth analysis is widely used to investigate electron-phonon coupling in semiconductor materials. As the temperature increases, the phonon population in the lattice increases, leading to enhanced carrier-phonon interactions and increased spectral broadening. The resulting linewidth broadening reflects the strength of electron-phonon coupling in the material. Therefore, the electron-phonon coupling strength can be evaluated from the temperature dependence of the full width at half maximum (FWHM) of the PL spectra using the following model [65–67]:

$$\Gamma(T) = \Gamma_0 + \Gamma_{ac} + \Gamma_{LO} + \Gamma_{imp} = \Gamma_0 + \gamma_{ac}T + \gamma_{LO}N_{LO}(T) + \gamma_{imp}e^{-E_b/k_BT} \tag{2.4}$$

Here, $\Gamma(T)$ represents the temperature-dependent PL linewidth, and Γ_0 is the temperature-independent inhomogeneous broadening caused by disorder and imperfections. Γ_{ac} and Γ_{LO} are homogeneous broadening terms resulting from acoustic phonon scattering and Fröhlich scattering, respectively, with carrier-phonon coupling strengths of γ_{ac} and γ_{LO}. $N_{LO}(T) = 1/(e^{E_{LO}/k_BT} - 1)$, where E_{LO} is the LO phonon energy and k_B is the Boltzmann

constant. Γ_{imp} represents the inhomogeneous broadening contribution induced by ionized impurities.

In hybrid perovskite materials, the contributions of acoustic phonon scattering and impurity scattering are often relatively weak at high temperatures and may be incorporated into Γ_0. As a result, the linewidth broadening can be simplified using the following expression [65]:

$$\Gamma(T) = \Gamma_0 + \gamma_{LO} N_{LO}(T) \tag{2.5}$$

Strong electron–phonon coupling generally leads to faster carrier relaxation, broader PL linewidths, and enhanced STE formation in quasi-2D perovskites.

Therefore, temperature-dependent PL linewidth analysis can be used to evaluate the electron-phonon coupling strength and STE-related relaxation behavior in the investigated quasi-2D perovskites.

2.4 Absorption Spectroscopy

Absorption spectroscopy provides direct information about the optical transitions and electronic structure of semiconductor materials. In quasi-2D perovskites, absorption measurements reveal excitonic absorption features, band-edge transitions, and the corresponding inorganic layer thicknesses.

Absorption spectroscopy was performed in reflection mode using a highly reflective reference mirror for background calibration. The measured reflectance was first normalized using the reference mirror. The normalized reflectance R can be expressed as

$$R = \frac{I}{I_0} \tag{2.6}$$

where I is the reflected light intensity from the sample and I_0 is the reflected light intensity from the reference mirror.

The absorbance is defined as the negative logarithm of the normalized intensity ratio:

$$A = -\log_{10}\left(\frac{I}{I_0}\right) \tag{2.7}$$

Therefore, using the normalized reflectance $R = I/I_0$, the absorption spectrum can be written as

$$A = -\log_{10}(R) \tag{2.8}$$

where A represents the absorbance obtained from the reflection-mode measurement.

In quasi-2D perovskites, characteristic excitonic absorption features are closely correlated with inorganic layer thickness and dimensionality of the materials. The absorption spectra were used to identify the characteristic excitonic absorption features of the quasi-2D perovskite single crystals and to support the assignment of the corresponding quasi-2D phases.

2.5 PL Spectroscopy

PL spectroscopy is a powerful technique for probing the optical and excited-state properties of semiconductor materials. In a PL process, electrons are excited from the valence band to the conduction band by external light excitation. Following carrier relaxation, radiative recombination between electrons and holes gives rise to photon emission. The emitted photon energy is related to the electronic structure of the material and can be expressed as

$$E = h\nu = \frac{hc}{\lambda} \tag{2.9}$$

where h is Planck's constant, ν is the photon frequency, c is the speed of light, and λ is the emission wavelength.

PL spectroscopy provides important information about bandgap energies, excitonic emission, defect-related emission, and carrier recombination pathways in perovskite materials [57]. In quasi-2D perovskites, PL measurements are widely used to investigate excitonic behaviors, electron-phonon interactions, and STE emission processes.

Temperature-dependent PL measurements provide insight into the thermal evolution of excited-state dynamics. Temperature-dependent variations in PL peak position, linewidth, and emission intensity can be used to evaluate exciton binding energies, carrier-phonon interactions, and thermal quenching processes. In particular, linewidth broadening analysis is commonly used to evaluate electron-phonon coupling strengths in perovskite systems.

2.6 TRPL Spectroscopy

TRPL spectroscopy enables direct investigation of excited-state dynamics and carrier relaxation processes in semiconductor materials. Compared with steady-state PL mea-

surements, TRPL measurements can provide time-dependent information about carrier recombination, exciton relaxation, and trapping processes in perovskite materials.

TRPL measurements were carried out using the time-correlated single photon counting (TCSPC) technique, which enables highly sensitive detection of photoluminescence signals at the single-photon level [68]. In the TCSPC system, the laser driver controls the pulsed excitation source and simultaneously provides a start signal to the detection electronics. After optical excitation, the emitted photons from the sample are detected by an avalanche photodiode (APD). Once the first emitted photon corresponding to one excitation pulse is detected, the system stops collecting the remaining photons from the same excitation cycle. The arrival time delay between the excitation pulse and the detected photon is then recorded in the corresponding time channel.

Repeating this process over many excitation cycles allows reconstruction of the time-dependent PL decay curve of the sample. The measured PL decay curves reflect the carrier recombination dynamics and excited-state relaxation processes in quasi-2D perovskites.

In this work, TRPL measurements were primarily used to compare the emitted photon counts under different excitation densities. The excitation power-dependent PL response was then analyzed using Eq. 2.3 to evaluate the dominant recombination behavior in the investigated quasi-2D perovskites.

2.7 TA Spectroscopy

TA spectroscopy is an ultrafast pump–probe technique capable of resolving excited-state dynamics and carrier relaxation processes in semiconductor materials [69]. As TA spectroscopy can directly monitor the ultrafast evolution of photoexcited carriers after optical excitation, it is particularly useful for investigating carrier relaxation pathways in perovskite materials.Compared with steady-state absorption spectroscopy, TA spectroscopy can provide time-resolved information about the evolution of excited states after photoexcitation.

In TA measurements, the sample is first excited by an ultrafast laser pulse referred to as the pump beam. After a controlled delay time, another broadband laser pulse known as the probe beam passes through the sample and is detected by the spectrometer system. The transient absorption signal is obtained from the difference between the probe absorption with and without pump excitation. Scanning the pump–probe delay time enables tracking of the temporal evolution of excited states.

The transient absorption signal can be expressed as

$$\Delta A = A_{\text{pump on}} - A_{\text{pump off}} \tag{2.10}$$

where $A_{\text{pump on}}$ and $A_{\text{pump off}}$ represent the absorbance measured with and without pump excitation, respectively.

Different transient absorption features in the ΔA spectra reflect distinct excited-state processes in perovskite materials. Negative ΔA signals generally originate from ground-state bleaching (GSB) and stimulated emission (SE), while positive ΔA signals are generally related to excited-state absorption (ESA). GSB originates from the depletion of ground-state carriers after photoexcitation. Stimulated emission typically appears near the PL emission region of the sample, whereas ESA corresponds to the further excitation of photoexcited carriers to higher-energy excited states.

Wavelength-dependent TA spectra reveal the evolution of different excited-state species and carrier relaxation pathways. Moreover, transient absorption decay dynamics as a function of pump-probe delay time can reveal the lifetimes and relaxation behaviors of excited states. TA spectroscopy is particularly suitable for studying carrier cooling, exciton relaxation, trap-assisted recombination, and STE-related dynamics in quasi-2D perovskites. Here, carrier cooling refers to the relaxation of hot carriers toward lower-energy band-edge states through phonon scattering.

Chapter 3

Experimental Method

This chapter describes the experimental procedures and optical characterization techniques used in this work. Absorption, PL, temperature-dependent PL, TRPL, and TA spectroscopy were employed to investigate the excited-state dynamics, carrier recombination processes, and electron-phonon interactions in the investigated perovskite systems.

The quasi-2D perovskite single crystals investigated in this study were synthesized by Dr. Mingli Liang. Assistance with temperature-dependent PL measurements was provided by Dr. Zehan Yao. Assistance with TA measurements was provided by Dr. Ahmed Magdy Kobaisy.

3.1 Synthesis of Quasi-2D Perovskite Single Crystals and Sample Preparation

$PbBr_2$ (98%), methylammonium bromide (MABr, 98%), iso-butylamine (iso-BA, 99%), n-butylamine (n-BA, 99.5%), n-pentylamine (n-PA, 99.5%), ethanol (99.8%), and hydrobromic acid (HBr, 47% in water) were used directly without additional purification. All chemicals were purchased from Sigma-Aldrich.

The long-chain amine bromide salts were first synthesized by adding stoichiometric amounts of iso-BA, n-BA, and n-PA into diluted aqueous HBr solution (25% in mixed ethanol and water) under vigorous stirring in an ice-water bath. The resulting white products were obtained after rotary evaporation at 60 °C. The resulting crystals of iso-BABr, n-BABr, and n-PABr were washed three times with ethanol and subsequently vacuum-dried for 24 h.

The quasi-2D perovskite single crystals investigated in this work, including n-PAPB ($n = 1$), n-PAPB ($n = 2$), iso-BAPB ($n = 2$), and n-BAPB ($n = 2$), were synthesized by Dr. Mingli Liang using a temperature-lowering crystallization method. The $n = 1$ and

$n = 2$ quasi-2D perovskite phases were obtained by adjusting the precursor stoichiometries corresponding to different inorganic layer thicknesses.

For the synthesis of the $n = 2$ quasi-2D RP perovskites, $PbBr_2$ (2.5 mmol), MABr (1.5 mmol), and the corresponding long-chain amine bromide salts (3.0 mmol) were dissolved in 5 mL HBr solution (47% in water) to form precursor solutions. The precursor mixtures were transferred into 20 mL glass bottles, sealed, and stirred at room temperature for 30 min to form yellow precipitates. Heating at 80 °C for several minutes yielded clear precursor solutions. Bulk single crystals were subsequently grown by slowly cooling the precursor solutions from 50 °C at a cooling rate of 0.5 °C/day.

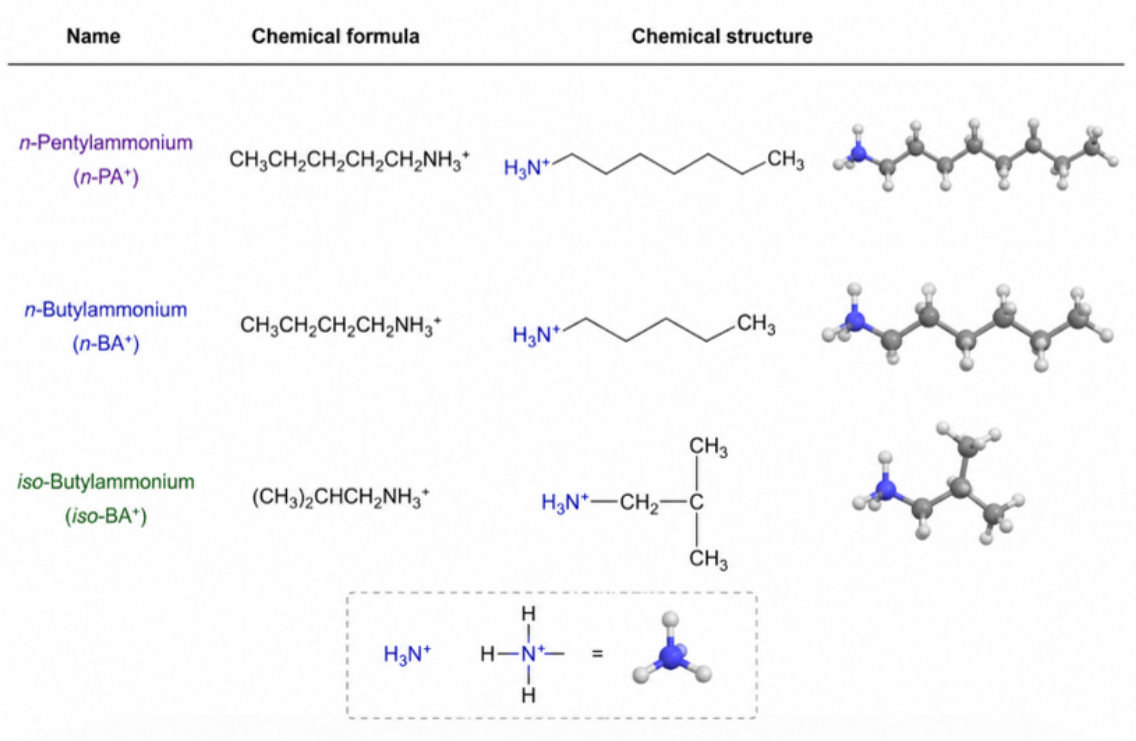

Figure 3.1: Organic spacer cations used in the quasi-2D perovskites.

Figure 3.1 presents the chemical structures of the organic spacer cations used in the investigated quasi-2D perovskites, including n-PA, n-BA and iso-BA. The three spacer cations differ primarily in carbon-chain length and molecular geometry. n-PA contains a longer linear alkyl chain compared with n-BA, while iso-BA possesses a branched molecular structure. These structural differences may influence lattice distortion, the dielectric environment, and quantum confinement behavior in quasi-2D perovskites.

For subsequent optical characterization measurements, the quasi-2D perovskite single crystals were fixed onto glass substrates for sample handling and optical measurements. Fig. 3.2 shows the quasi-2D perovskite single crystal samples investigated in this work, including n-PAPB ($n = 1$), n-PAPB ($n = 2$), iso-BAPB ($n = 2$), and n-BAPB ($n = 2$).

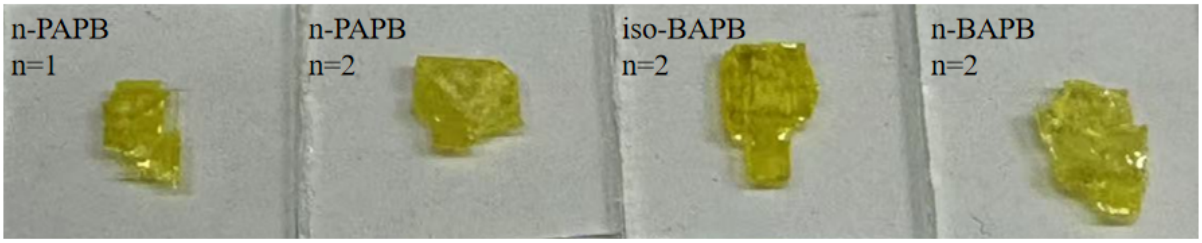

Figure 3.2: Quasi-2D perovskite single crystal samples.

3.2 Optical Characterization

A combination of optical spectroscopy techniques was used to characterize the photophysical properties and excited-state dynamics of the quasi-2D perovskite single crystals. Absorption spectroscopy, PL spectroscopy, temperature-dependent PL spectroscopy, TRPL spectroscopy, and TA spectroscopy were used to study the optical transitions, carrier recombination processes, electron-phonon interactions, and ultrafast excited-state relaxation behaviors of the investigated perovskite systems.

3.2.1 Absorption Spectroscopy

Ultraviolet-visible (UV-Vis) absorption spectroscopy is widely used to investigate the optical properties and electronic transitions of semiconductor materials. In the ultraviolet and visible spectral regions, photon absorption induces electronic transitions from lower-energy states to higher-energy states, resulting in characteristic absorption features.

In this work, absorption measurements were performed using the reflection module of a PerkinElmer Lambda 1050 UV-Vis spectrophotometer. The core component of the reflection module is an integrating sphere, as shown in Fig. 3.3. For the measurements, the quasi-2D perovskite single crystals were mounted inside the sample chamber on the right side of the integrating sphere and fixed onto a highly reflective reference substrate corresponding to 100% reflectance.

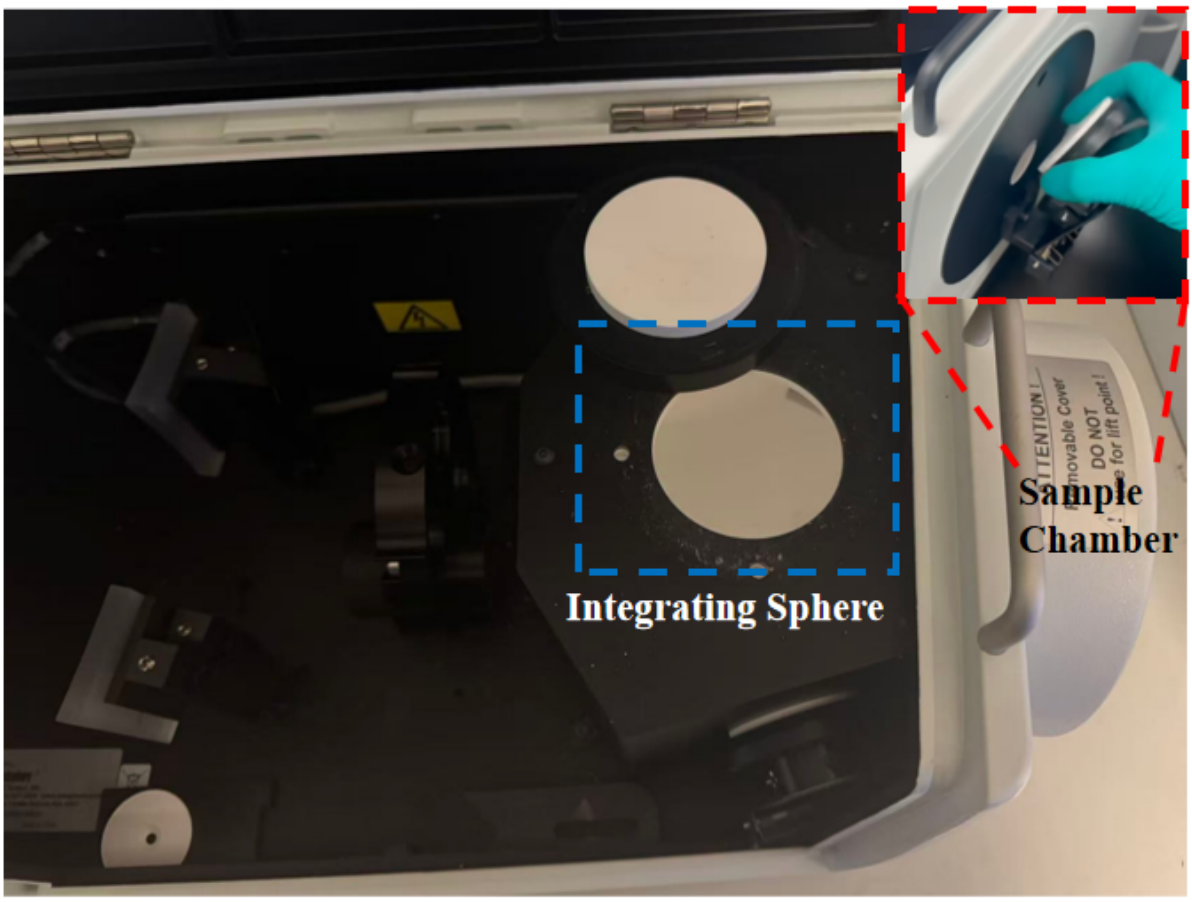

Figure 3.3: The reflection module of the PerkinElmer Lambda 1050 UV-Vis spectrophotometer.

Before sample characterization, a reference spectrum was first collected using the reflective reference substrate. The reflected intensity from the sample was then measured and normalized using the reference signal according to the previously introduced relationship $R = I/I_0$. The absorbance was subsequently calculated from the normalized reflectance using $A = -\log_{10}(R)$.

The absorption spectra were used to identify the characteristic excitonic absorption features of the quasi-2D perovskite single crystals and to distinguish the corresponding $n = 1$ and $n = 2$ phases.

3.2.2 PL Spectroscopy

PL measurements were performed using a HORIBA Fluorolog-3 spectrofluorometer system, as shown in Fig. 3.4. During the measurements, the quasi-2D perovskite single crystals were placed inside the sample chamber. Depending on the crystal surface quality, the PL signals were collected either along the surface normal direction or in a right-angle collection geometry perpendicular to the excitation beam.

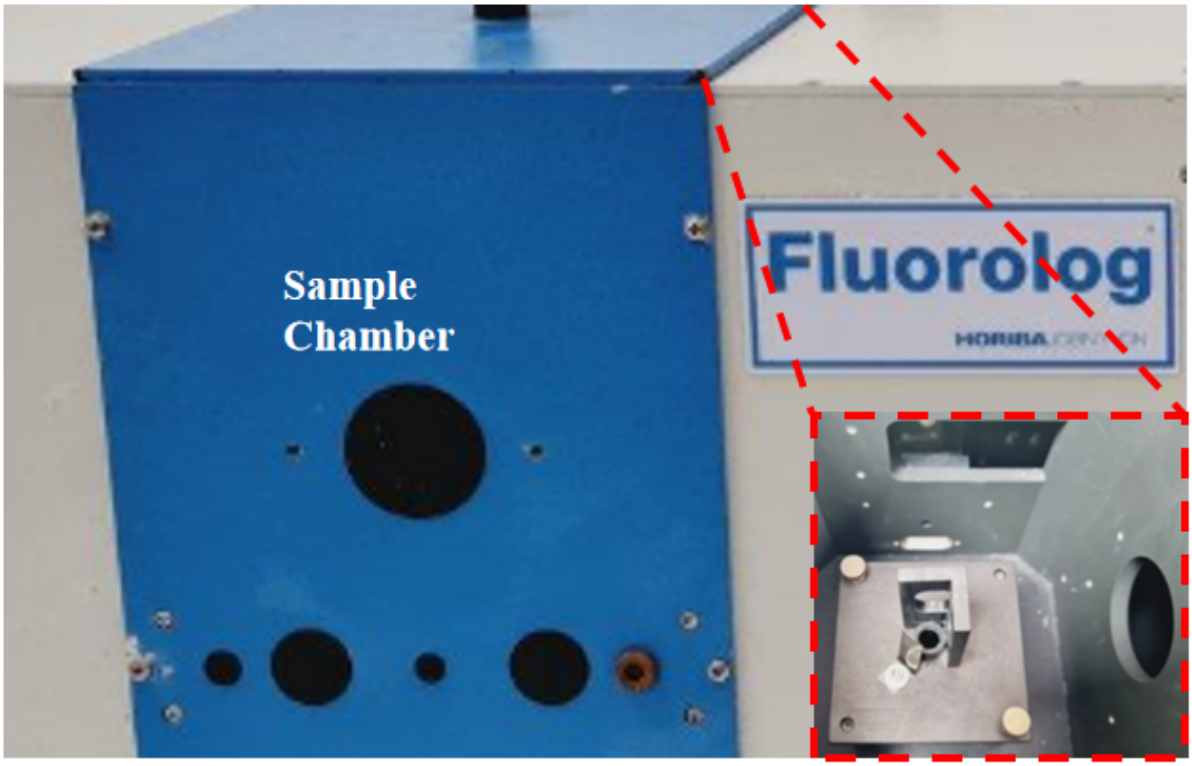

Figure 3.4: HORIBA Fluorolog-3 spectrofluorometer.

In the measurements, an excitation wavelength of 335 nm was selected because the PL emission of the investigated quasi-2D perovskite crystals was mainly located around 500 nm. Special attention was paid to minimizing interference from Raman scattering and second-order scattering signals. The Raman scattering peak shifts with the excitation wavelength and was observed around 400 nm under 335 nm excitation. Moreover, second-order scattering artifacts may appear near twice the excitation wavelength, corresponding to approximately 670 nm in the present measurements. Therefore, these spectral regions were excluded during the analysis of the PL emission spectra.

3.2.3 Temperature-dependent PL Spectroscopy

Temperature-dependent PL measurements were performed using the same HORIBA Fluorolog-3 spectrofluorometer system. To obtain PL spectra between 100 K and 300 K with a temperature interval of 10 K, a low-temperature chamber was employed, as shown in Fig. 3.5(b). The quasi-2D perovskite single crystals were fixed using the sample holder shown in the figure and placed inside the sample chamber at the bottom of the cryogenic system.

Before cooling, the low-temperature chamber was evacuated using the vacuum pump shown in Fig. 3.5(a). The chamber pressure was reduced to approximately 10^{-5} mbar in order to reduce thermal convection and avoid condensation during low-temperature

measurements.

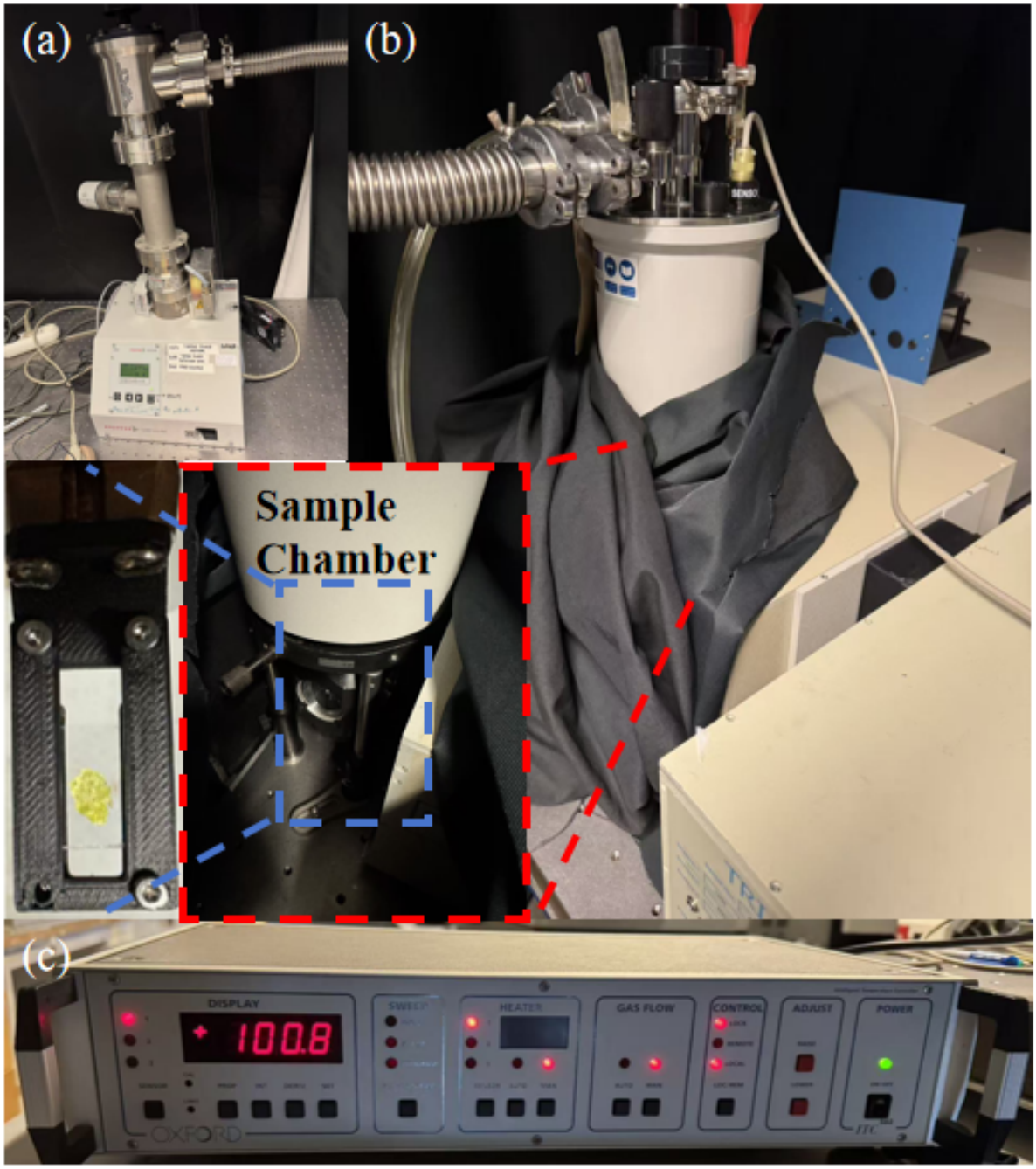

Figure 3.5: Experimental setup for temperature-dependent PL measurements.

The cryogenic chamber temperature was controlled through a dynamic balance between liquid nitrogen cooling and internal resistive heating. Liquid nitrogen was introduced from the top of the chamber to cool the sample region, while the temperature was gradually adjusted using an internal heating rod. The corresponding temperature control module is shown in Fig. 3.5(c). During the measurements, the system was first cooled down to 100 K and subsequently heated slowly to 300 K for temperature-dependent PL characterization.

3.2.4 TRPL Spectroscopy

TRPL measurements were performed using a TCSPC system. The time resolution of a TCSPC system is primarily determined by its instrument response function, which is mainly limited by the response speed of the photodetector [70]. In addition, the excitation source and the timing jitter of the electronic components may further broaden the instrument response function.

In this work, the samples were excited using a pulsed diode laser externally triggered at 2.5 MHz. The excitation wavelength was 375 nm and the pulse duration was approximately 200 ps. The setup included a picosecond pulsed driver (PicoQuant PDL 828 "Sepia II"), a pulsed laser source, and a picosecond event timer (PicoQuant PicoHarp 300), as shown in Fig. 3.6. The emitted photons were detected using a fast single-photon avalanche photodiode (SPAD, Micro Photon Device) with a response time below 50 ps after passing through a 500 nm long-pass optical filter.

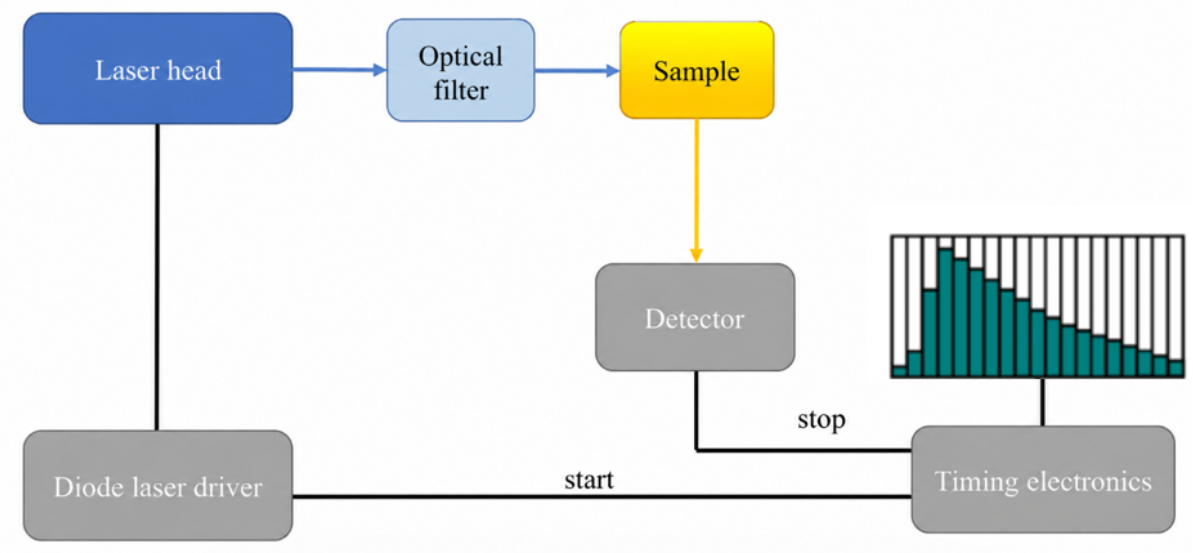

Figure 3.6: Experimental setup for fluorescence decay measurements with TCSPC.

Neutral-density filters with different optical densities (ODs) were also used to control the excitation intensity during the measurements. By varying the OD values, different excitation photon densities were obtained, and the corresponding emitted PL photon intensities were measured for power-dependent analysis.

The TCSPC measurements provide information about various excited-state processes, including carrier lifetimes, recombination pathways, and relaxation processes in semiconductor materials. The TCSPC system was primarily employed to investigate the excitation power-dependent PL response by measuring the emitted photon counts under different excitation densities. The power-dependent PL data were subsequently used to analyze

the recombination behavior of the quasi-2D perovskite systems.

3.2.5 TA Spectroscopy

TA spectroscopy is an ultrafast pump–probe technique commonly used to investigate excited-state dynamics and carrier relaxation processes in semiconductor materials. In a typical TA measurement, the sample is first excited by an ultrafast laser pulse referred to as the pump beam. The transient absorption changes of the delayed probe beam are then detected as a function of pump–probe delay time. [69].

The TA spectrum is obtained from the difference between the probe absorption signals measured with and without pump excitation. In the experiment, the pump-on and pump-off states were achieved using a mechanical chopper to periodically block the pump beam. Varying the delay time between the pump and probe beams enables TA spectra with both temporal and spectral resolution to be obtained. The transient absorption signal can be expressed as

$$\Delta A = A_{\text{pump on}} - A_{\text{pump off}} \tag{3.1}$$

In this work, TA measurements were performed using a femtosecond pump-probe setup, as shown in Fig. 3.7. Laser pulses with a central wavelength of 800 nm, pulse duration of approximately 60-80 fs, and repetition rate of 1 kHz were generated by a regenerative amplifier (Spitfire XP Pro, Spectra Physics) seeded by a femtosecond oscillator (Mai Tai SP, Spectra Physics). The fundamental laser beam was split into pump and probe beams for the TA measurements.

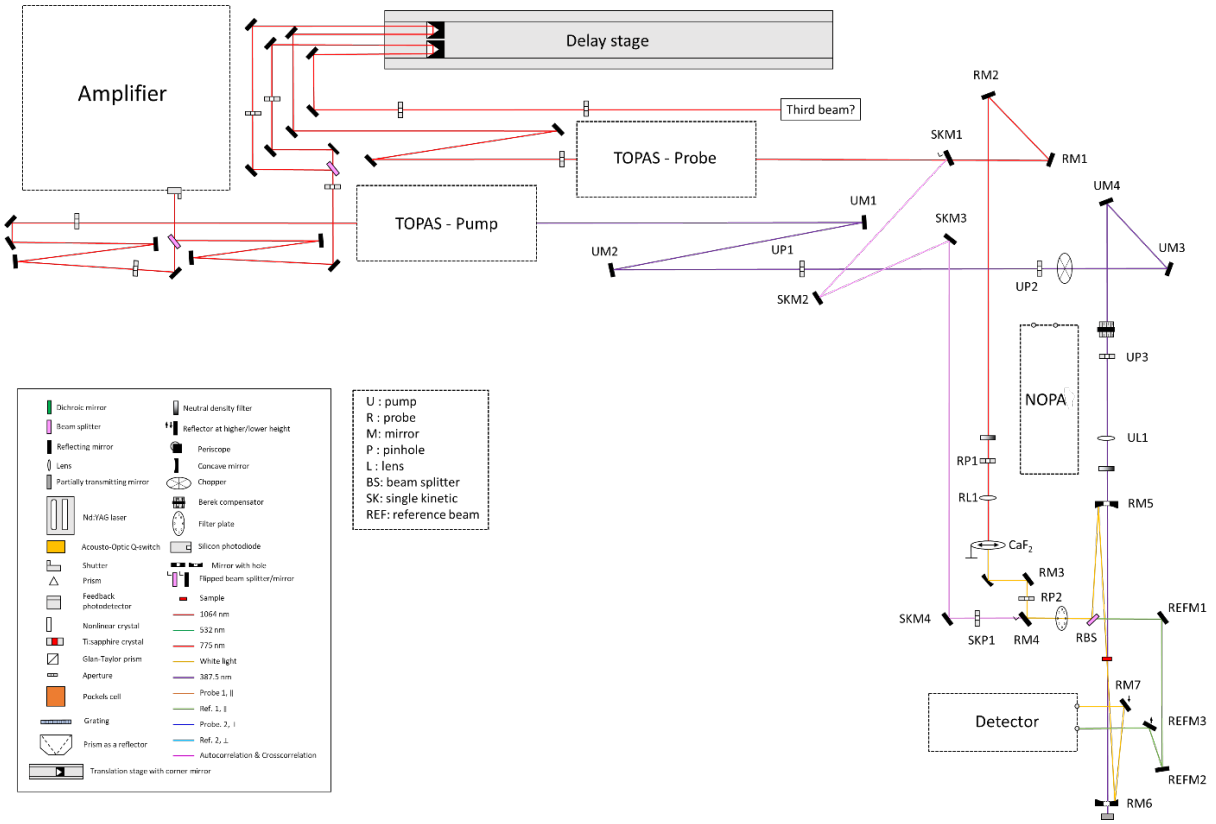

Figure 3.7: Schematic of TA spectroscopy setup.

The pump beam at 400 nm was generated through second-harmonic generation using a beta barium borate (BBO) crystal. The probe beam was generated through supercontinuum white-light generation in a CaF_2 crystal. A mechanical delay stage was employed to control the temporal delay between the pump and probe beams. Notably, a Berek compensator was inserted into the pump beam path to establish the magic-angle (54.7°) polarization condition between the pump and probe beams, thereby minimizing polarization-dependent effects during the measurements [71].

For the TA measurements, the average pump power density was approximately 0.4 W/cm^2. The corresponding pulse energy density was approximately 0.1 mJ/cm^2. The sample position was kept fixed, and several thousand pump–probe scans were averaged at the same position to improve the signal-to-noise ratio. The probe signals were detected using a broadband detection system consisting of a monochromator and a diode-array detector, while photodetectors were additionally used for synchronization and reference signal collection.

Chapter 4

Results and Discussion

This chapter presents the optical properties and excited-state dynamics of the investigated quasi-2D perovskite single crystals. Steady-state absorption and PL spectra are first analyzed to identify the main optical transitions and mixed-phase characteristics. Excitation power-dependent PL measurements are then used to evaluate the dominant recombination behavior. Temperature-dependent PL spectroscopy is applied to examine carrier localization and electron-phonon coupling. Finally, TA spectroscopy is used to probe ultrafast relaxation and the formation of localized excited states.

4.1 Absorption and Photoluminescence Properties

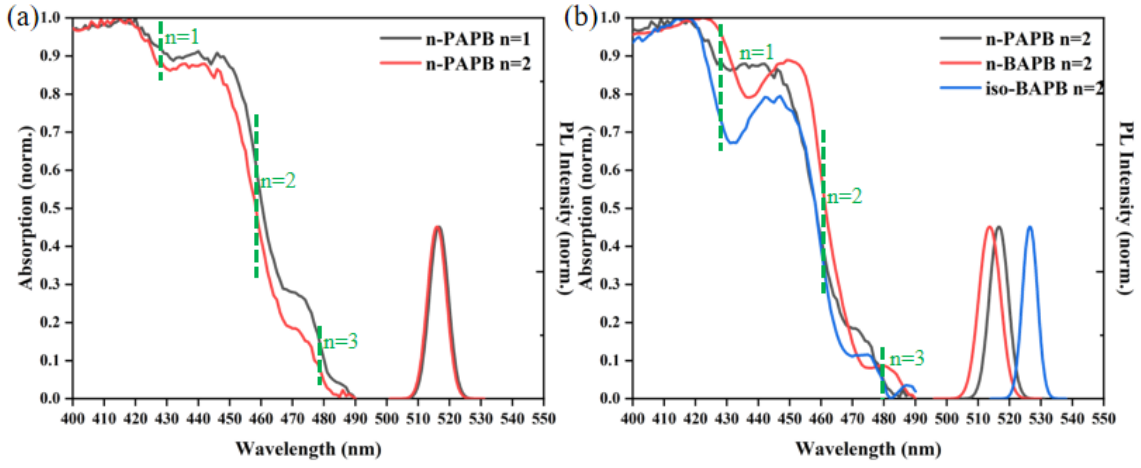

Figure 4.1: Steady-state absorption spectra and PL spectra of quasi-2D perovskite single crystals.

Fig. 4.1 (a) shows the absorption and PL spectra of the n-PAPB samples with nominal $n = 1$ and $n = 2$ compositions. Several characteristic absorption peaks can be observed at

approximately 425 nm, 460 nm, and 480 nm, while the main PL emission peak is located around 516 nm. The overall spectral features of the two samples are relatively similar, indicating that both samples exhibit mixed-phase characteristics rather than pure single-n phases.

According to previous studies on quasi-2D Ruddlesden-Popper perovskites, the absorption peak near 415 nm is commonly assigned to the $n = 1$ phase, while the peaks around 460 nm and 480 nm are associated with the $n = 2$ and $n = 3$ phases [72]. The coexistence of multiple excitonic absorption peaks suggests the simultaneous presence of different inorganic layer thicknesses within the investigated crystals. Such mixed-phase behavior is frequently observed in quasi-2D perovskite film systems because of the thermodynamic and kinetic instability of individual n-phases during crystal growth.

The PL emission peak centered at approximately 516 nm lies between the reported emission energies of low-n quasi-2D perovskites and bulk-like 3D bromide perovskites [56, 72]. This behavior is characteristic of quasi-2D perovskite systems, where energy transfer processes can occur from smaller-n phases with larger bandgaps toward larger-n phases with smaller bandgaps. As a result, although the precursor stoichiometries were designed to synthesize nominal $n = 1$ and $n = 2$ samples, the measured optical spectra indicate that both samples mainly behave as mixed-phase quasi-2D perovskites containing multiple n-values, including $n = 1$, $n = 2$, and $n = 3$ domains.

Fig. 4.1 (b) compares the absorption and PL spectra of quasi-2D perovskite samples with different organic spacer cations. Similar to the n-PAPB samples discussed above, several excitonic absorption features can still be observed, indicating the coexistence of multiple n-phases, including $n = 1$, $n = 2$, and $n = 3$ domains. This suggests that the mixed-phase behavior is not limited to a single spacer system, but is a common feature in the investigated quasi-2D perovskite crystals.

In contrast to the similar absorption features, the PL emission peaks show clear spacer-dependent differences. The main emission peaks of n-BAPB, n-PAPB, and iso-BAPB are located at approximately 510 nm, 516 nm, and 526 nm, respectively. This gradual redshift suggests that the organic spacer cations can influence the emission properties even when the absorption spectra exhibit similar mixed-phase characteristics. One possible explanation is that the spacer molecules modify the local inorganic framework, such as the Pb-Br bond lengths or bond angles within the octahedral network, thereby altering the bandgap energy. Alternatively, the redshifted emission may be associated with STE emission, which is strongly influenced by electron-phonon coupling and lattice softness that can also be modulated by the organic spacer cations.

The difference in PL emission can be related to the molecular structure of the organic spacer cations. n-BA and n-PA are linear alkylammonium spacers, while iso-BA has a

branched structure. The longer linear chain in n-PA may increase the interlayer spacing and modify the dielectric environment compared with n-BA, leading to a slight redshift of the emission peak. In contrast, the branched iso-BA spacer can introduce different steric effects and molecular packing behavior, which may induce stronger lattice distortion or exciton localization. These structural effects can further modify the local electronic environment and result in the most pronounced redshift among the three samples.

Therefore, although all three samples show mixed-n quasi-2D characteristics in their absorption spectra, their PL emission behavior is strongly affected by the organic spacer cations. The observed emission trend suggests that spacer molecular geometry plays an important role in tuning the photophysical properties of quasi-2D perovskite single crystals.

4.2 Excitation Power-dependent Photoluminescence

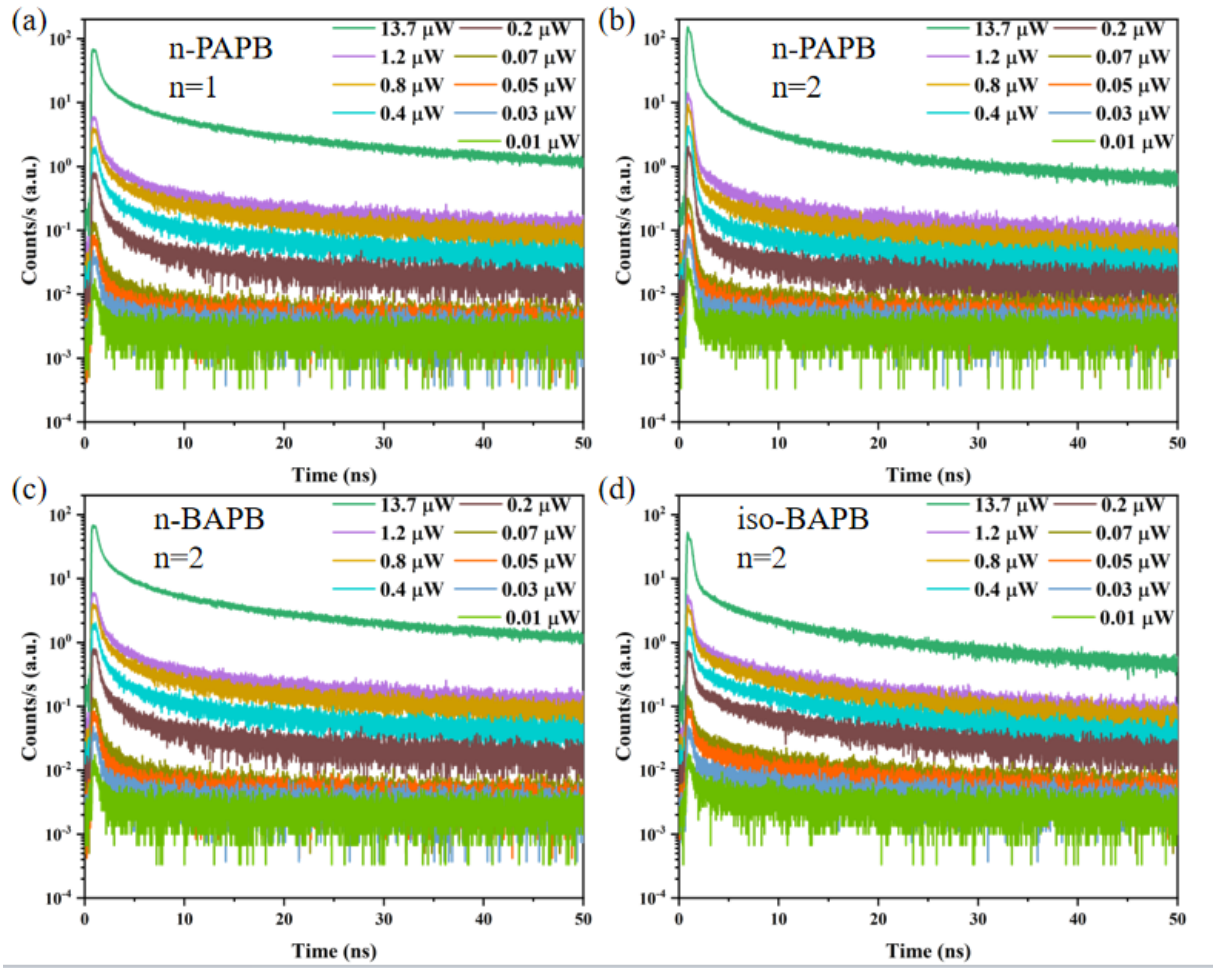

Figure 4.2: TRPL spectra of quasi-2D perovskite single crystals under different excitation powers.

Fig. 4.2 (a)-(d) show the TRPL signals of the four investigated quasi-2D perovskite samples measured under different excitation powers. For all samples, the detected PL photon counts increase systematically with increasing excitation intensity, indicating enhanced radiative recombination under higher excitation densities. The overall decay profiles remain similar at different excitation powers, suggesting that the dominant recombination mechanism does not change significantly within the investigated excitation range.

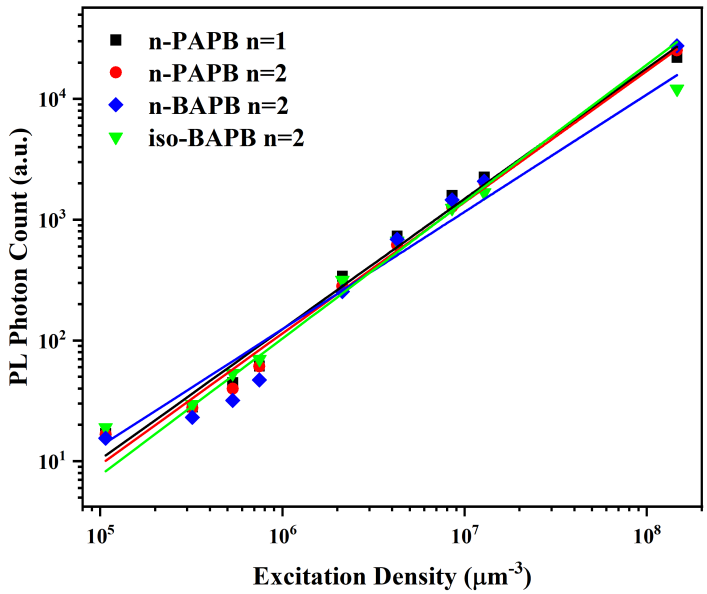

Figure 4.3: Power-dependent PL intensity fitting of quasi-2D perovskite single crystals.

To further investigate the recombination behavior of the excited states, the integrated PL photon counts extracted from the TRPL measurements were plotted as a function of excitation photon counts, as shown in Fig. 4.3. The relationship between PL intensity and excitation density was analyzed using the power-law relationship

$$I_{PL} \propto P^k \tag{4.1}$$

where I_{PL} is the integrated PL intensity, P is the excitation photon count, and k is the power-law coefficient.

The fitted k values for n-PAPB ($n = 1$), n-PAPB ($n = 2$), n-BAPB ($n = 2$), and iso-BAPB ($n = 2$) are summarized in Table 4.1. The obtained values are 1.07931, 1.08643, 1.13296, and 0.97106, respectively. All fitted k values remain close to 1, indicating that the PL intensity exhibits an approximately linear dependence on the excitation density. Such behavior is characteristic of monomolecular recombination processes and is commonly associated with excitonic radiative recombination in quasi-2D perovskite systems.

Table 4.1: Fitted power-law coefficients of the investigated quasi-2D perovskites.

Sample	k value
n-PAPB ($n = 1$)	1.07931
n-PAPB ($n = 2$)	1.08643
n-BAPB ($n = 2$)	1.13296
iso-BAPB ($n = 2$)	0.97106

Among the investigated samples, iso-BAPB exhibits a k value closest to unity, suggesting relatively ideal excitonic recombination behavior with weaker influence from higher-order recombination processes. In contrast, the slightly larger k values observed in n-PAPB and n-BAPB may indicate weak contributions from additional carrier interactions or trap-assisted recombination channels under higher excitation densities. Nevertheless, the relatively small variation among the fitted k values suggests that excitonic recombination dominates the PL processes in all four investigated quasi-2D perovskite crystals, which is consistent with previous reports on excitonic recombination behaviors in lead halide perovskites [73]. Furthermore, the excitation density used in the present measurements remains within the low-density excitation region, where linear excitonic recombination is expected to dominate. No clear signatures of higher-order multiexciton processes, such as Auger recombination, were observed under the investigated excitation conditions.

4.3 Temperature-dependent Photoluminescence Properties

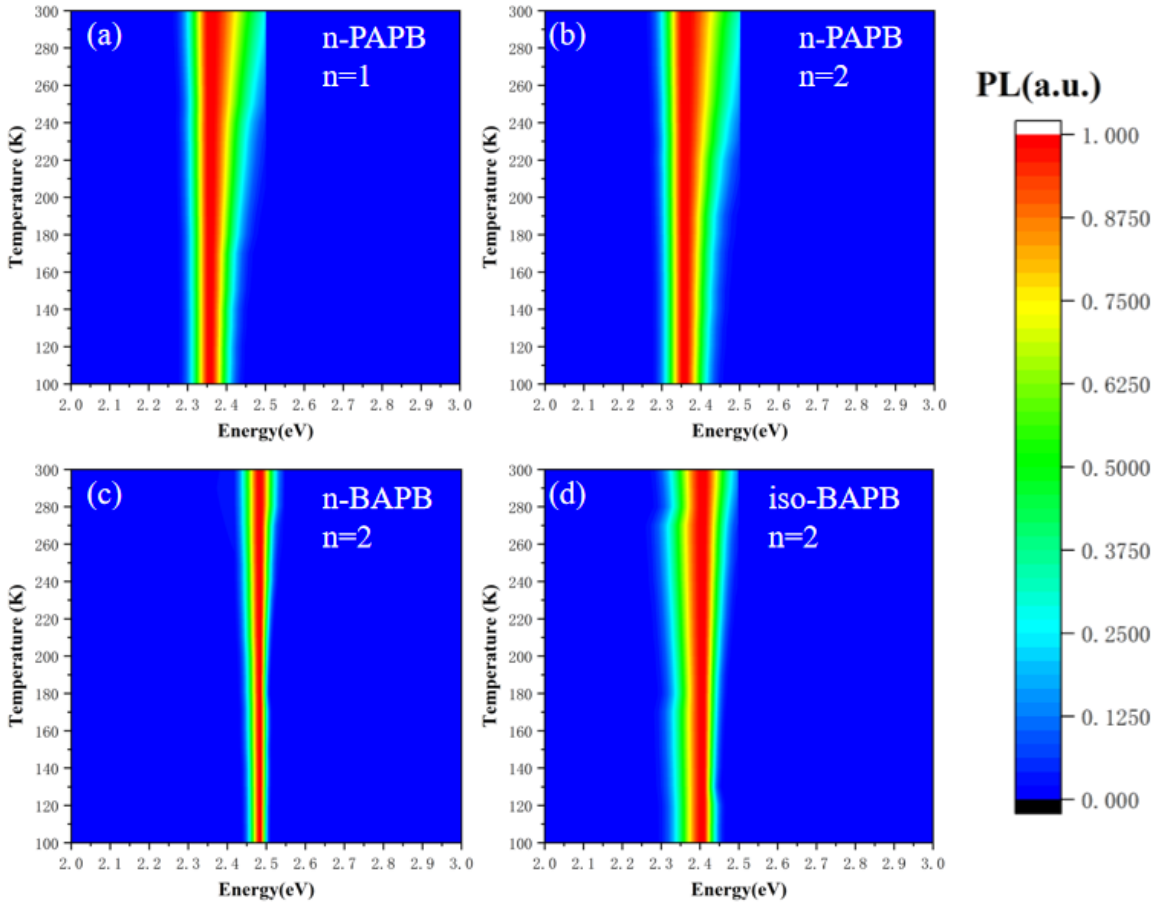

Figure 4.4: Temperature-dependent PL contour maps of quasi-2D perovskite single crystals.

Figure 4.4 shows the temperature-dependent PL contour maps of the investigated quasi-2D perovskite single crystals measured from 100 K to 300 K. For all samples, the PL linewidth gradually increases with increasing temperature because higher phonon populations at elevated temperatures enhance carrier-phonon scattering and accelerate the dephasing of the excited states, resulting in spectral broadening.

The PL peak positions of the different samples remain relatively stable within the investigated temperature range, while slight redshifts and linewidth broadenings can still be observed at higher temperatures. Such behavior is commonly attributed to increased electron-phonon coupling and thermally activated lattice vibrations in quasi-2D perovskite systems.

Compared with n-PAPB and n-BAPB, the iso-BAPB sample exhibits a broader emission distribution and more pronounced low-energy spectral broadening at elevated tempera-

tures. This behavior may indicate stronger exciton localization and enhanced STE-related emission in the iso-BAPB crystal. The branched organic spacer in iso-BAPB could induce larger lattice distortion and stronger carrier localization, thereby stabilizing STE-related states through enhanced exciton-phonon coupling.

In contrast, the relatively narrower emission features observed in n-PAPB and n-BAPB suggest comparatively weaker localization effects and more dominant free-excitonic radiative recombination.

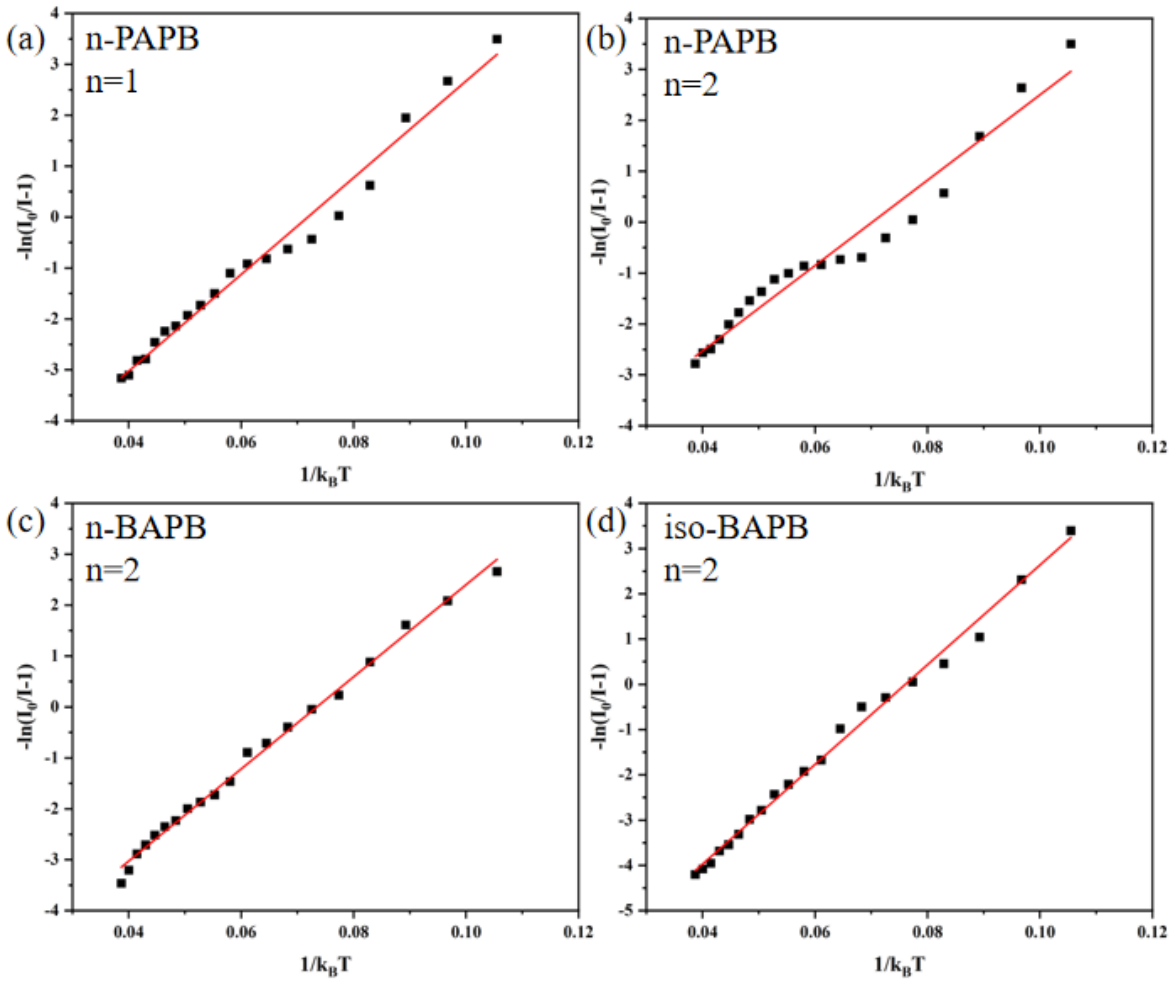

Figure 4.5: $-\ln[(I_0/I(T)) - 1]$ vs. $1/k_BT$ plots of the investigated quasi-2D perovskite single crystals for exciton binding energy fitting.

The exciton binding energies (E_b) of the investigated quasi-2D perovskite crystals were estimated from the temperature-dependent PL intensities using an Arrhenius-type fitting model [28, 55, 56]:

$$I(T) = \frac{I_0}{1 + A\exp(-E_b/k_BT)} \tag{4.2}$$

where $I(T)$ and I_0 represent the integrated PL intensities at temperature T and 100 K, A is a fitting constant, k_B is the Boltzmann constant, and E_b is the exciton binding energy.

Figure 4.5 shows the corresponding fitting results for the four investigated samples. The extracted E_b values for n-PAPB ($n = 1$), n-PAPB ($n = 2$), n-BAPB ($n = 2$), and iso-BAPB ($n = 2$) are 95 meV, 84 meV, 90 meV, and 110 meV, respectively. These values are summarized in Table 4.2.

The obtained exciton binding energies are significantly larger than those typically reported for conventional 3D perovskites, which are usually around 60 meV or lower [56], and are comparable to the values commonly reported for quasi-2D lead halide perovskites, which are typically around 100 meV or higher [74]. The relatively large E_b values indicate enhanced dielectric and quantum confinement effects in the investigated quasi-2D systems, which can stabilize excitonic states at room temperature. Among the investigated samples, iso-BAPB exhibits the largest exciton binding energy, suggesting stronger exciton localization. This observation is also consistent with the broader temperature-dependent PL features discussed previously.

Table 4.2: Extracted exciton binding energies of the investigated quasi-2D perovskites.

Sample	E_b (meV)
n-PAPB ($n = 1$)	95
n-PAPB ($n = 2$)	84
n-BAPB ($n = 2$)	90
iso-BAPB ($n = 2$)	110

The temperature-dependent PL linewidths of the investigated quasi-2D perovskite crystals were further analyzed in order to evaluate the electron-phonon coupling strengths. The FWHM values extracted from the PL spectra were fitted using the temperature-dependent broadening model [65–67]:

$$\Gamma(T) = \Gamma_0 + \gamma_{LO} N_{LO}(T) \tag{4.3}$$

where $\Gamma(T)$ is the PL linewidth at temperature T, Γ_0 is the temperature-independent inhomogeneous broadening term, γ_{LO} represents the exciton-LO phonon coupling strength, and $N_{LO}(T)$ is the Bose-Einstein occupation number of LO phonons:

$$N_{LO}(T) = \frac{1}{\exp(E_{LO}/k_B T) - 1} \tag{4.4}$$

Here, E_{LO} is the LO phonon energy and k_B is the Boltzmann constant.

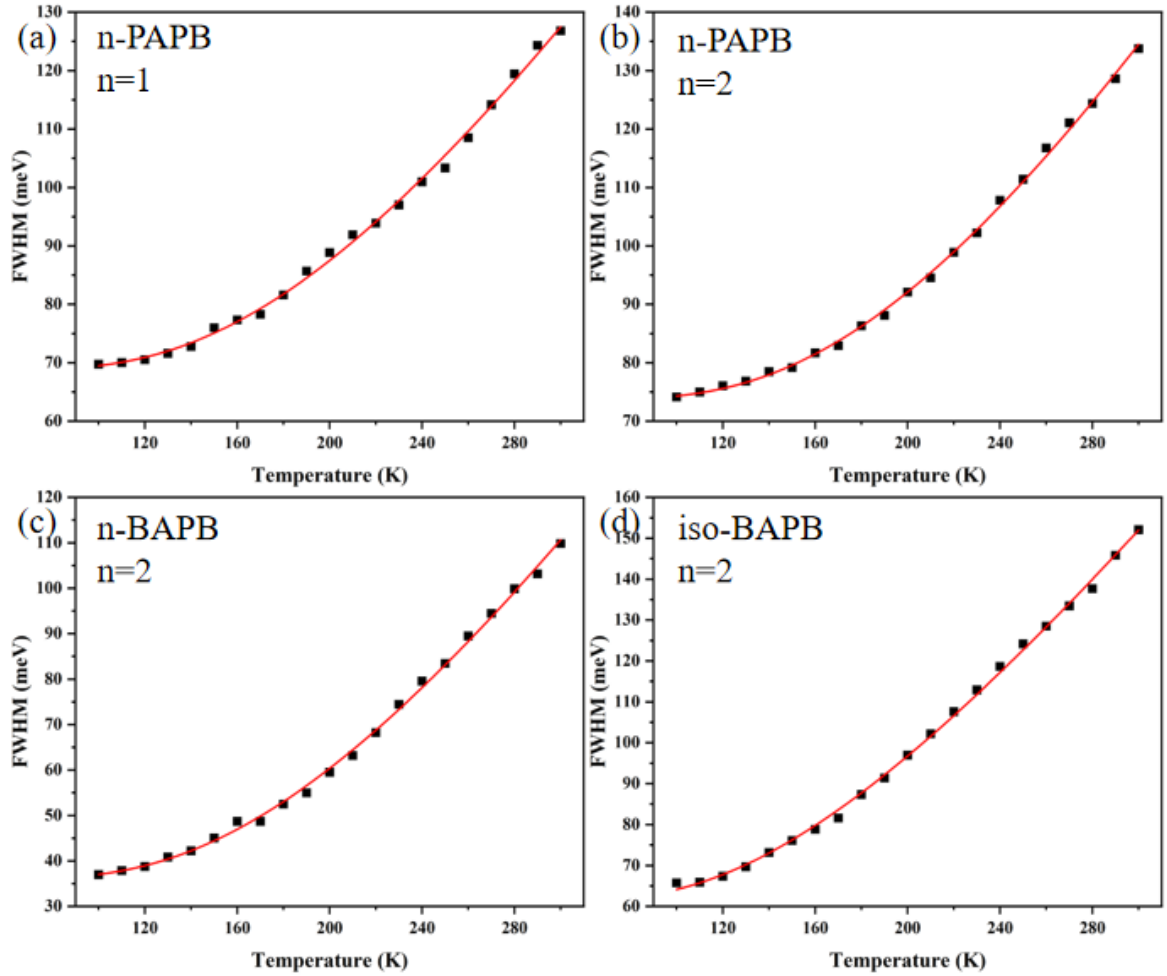

Figure 4.6: Temperature-dependent PL linewidth fitting of quasi-2D perovskite single crystals using the electron-phonon coupling model.

Figure 4.6 shows the corresponding fitting results of the temperature-dependent PL linewidths for the four investigated samples. The extracted fitting parameters are summarized in Table 4.3. The obtained Γ_0 values are 68 meV, 73 meV, 35 meV, and 61 meV for n-PAPB ($n = 1$), n-PAPB ($n = 2$), n-BAPB ($n = 2$), and iso-BAPB ($n = 2$), respectively.

Table 4.3: Fitted parameters of temperature-dependent PL linewidth broadening.

Sample	Γ_0 (meV)	γ_{LO} (meV)	E_{LO} (meV)
n-PAPB ($n = 1$)	68	526	54
n-PAPB ($n = 2$)	73	507	57
n-BAPB ($n = 2$)	35	510	53
iso-BAPB ($n = 2$)	61	368	42

The extracted exciton-LO phonon coupling strengths (γ_{LO}) are 526 meV, 507 meV, 510 meV, and 368 meV for n-PAPB ($n = 1$), n-PAPB ($n = 2$), n-BAPB ($n = 2$), and iso-BAPB

($n = 2$), respectively, while the corresponding LO phonon energies (E_{LO}) are 54 meV, 57 meV, 53 meV, and 42 meV. The extracted fitting parameters reveal noticeable differences in the electron-phonon coupling behaviors among the investigated quasi-2D perovskite crystals. The relatively large γ_{LO} values observed in n-PAPB ($n = 1$), n-PAPB ($n = 2$), and n-BAPB ($n = 2$) indicate strong coupling between excitons and LO phonons, which can enhance carrier localization, facilitate lattice distortion under photoexcitation, and promote the formation of STEs, resulting in redshifted emission. Strong γ_{LO} values are generally associated with more pronounced exciton self-trapping processes and stronger carrier-phonon interactions, which may promote localized radiative recombination and increase the contribution of STE emission in quasi-2D perovskite materials.

In contrast, iso-BAPB exhibits a smaller γ_{LO} value of 368 meV together with the lowest E_{LO} value of 42 meV. The reduced E_{LO} suggests softer lattice vibrations and modified phonon dynamics induced by the branched iso-BA spacer. Meanwhile, the broader PL linewidth observed in the temperature-dependent spectra indicates enhanced fluctuations in the emission energy arising from carrier-phonon interactions. Such fluctuations can contribute to spectral broadening even in systems with relatively weaker overall electron-phonon coupling.

Furthermore, the relatively large zero-temperature linewidth broadening term Γ_0 observed in n-PAPB ($n = 1$) and n-PAPB ($n = 2$) suggests stronger static inhomogeneous broadening, which may originate from phase heterogeneity and local disorder in the mixed-phase quasi-2D structures. Such inhomogeneous broadening can affect spectral purity and carrier transport properties in optoelectronic devices. In comparison, the smaller Γ_0 value observed in n-BAPB indicates relatively reduced static disorder and narrower intrinsic linewidth broadening, which may be beneficial for stable optical emission and improved spectral performance in light-emitting applications.

Overall, the differences in Γ_0, γ_{LO}, and E_{LO} demonstrate that the organic spacer structure can strongly influence lattice dynamics, carrier-phonon interactions, and exciton localization in quasi-2D perovskites. These factors are closely related to the optical stability, emission efficiency, and carrier relaxation behaviors of perovskite-based LEDs and other optoelectronic devices.

4.4 TA Dynamics

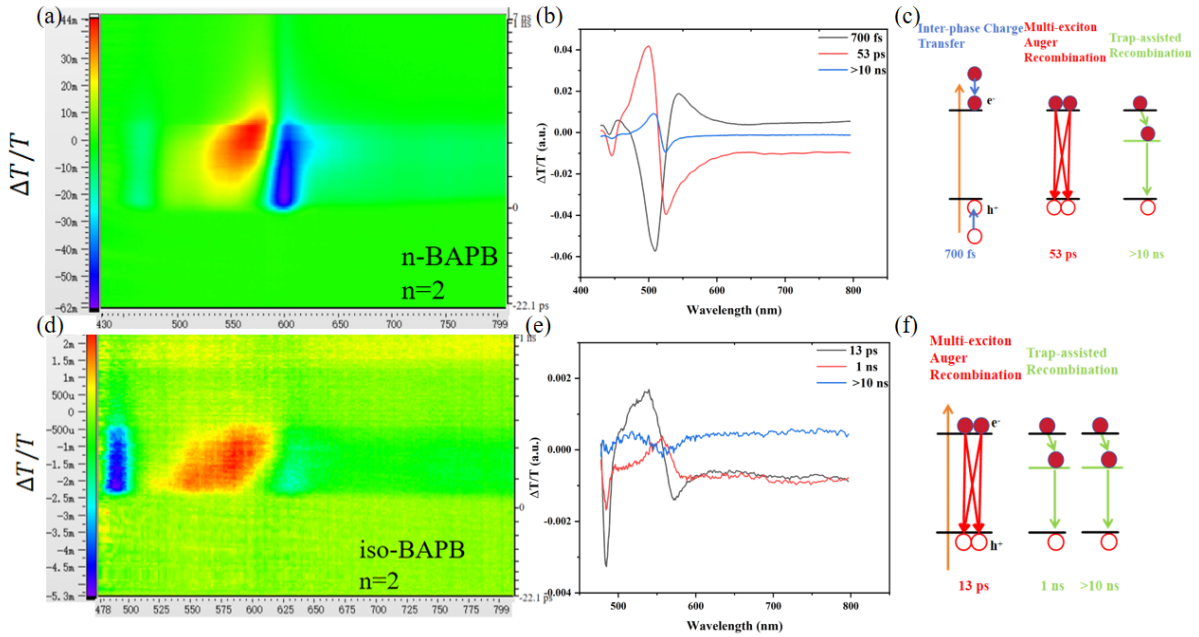

Figure 4.7: TA spectra and decay dynamics of n-BAPB and iso-BAPB quasi-2D perovskite single crystals.

The ultrafast carrier dynamics of the investigated quasi-2D perovskite single crystals were further studied by femtosecond TA spectroscopy. Fig. 4.7 (a,d) show the TA contour maps of n-BAPB and iso-BAPB crystals, respectively, while Fig. 4.7 (b,e) present the transient spectra extracted at representative delay times. Owing to the degradation of the n-PAPB crystal during the long-time measurements, reliable TA data could not be obtained for this sample.

For both n-BAPB and iso-BAPB crystals, strong negative transient signals are observed near the band-edge region around 500-530 nm immediately after photoexcitation. These negative features are mainly attributed to GSB caused by state filling of the band-edge excitonic states. Furthermore, positive transient signals appearing at longer wavelengths are assigned to ESA, indicating the possibility of optical transitions of excited species to higher excited states. To further analyze the ultrafast carrier relaxation dynamics, singular value decomposition (SVD) fitting was performed on the transient absorption datasets. SVD fitting decomposes the transient absorption data into several characteristic spectral components with corresponding decay lifetimes, allowing the dominant relaxation processes to be identified. Therefore, the extracted spectra shown in Fig. 4.7(b,e) represent the SVD-fitted decay-associated spectral components with corresponding lifetimes, rather than transient spectra at specific time delays.

For the n-BAPB crystal, the fast decay associate spectral component with a lifetime of 700

fs exhibits strong mirroring feature of ESA and band edge GSB features, suggesting rapid population of band-edge excitonic states after excitation and hot carrier cooling or charge transfer from high n phase to low n phase. In the second component with lifetime of 53 ps, it mainly reflects the decay of ESA and GSB due to the multi-exciton Auger recombination process under relatively high excitation conditions. The blue component is assigned to a long-lived component with lifetime longer than the experimental time window (>10 ns), which is attributed to the intrinsic radiative and nonradiative recombination of single STEs.

In the iso-BAPB crystal, no distinct femtosecond component can be clearly resolved, suggesting that the carrier cooling or STE formation process occurs within the instrumental response time. The transient spectrum at 13 ps exhibits pronounced GSB features together with broad ESA signals, while the ESA contribution decreases significantly at 1 ns. The 13 ps component is also attributed to the multi-exciton Auger recombination process. The relatively faster Auger recombination process in iso-BAPB suggests that the softer lattice induced by the branched iso-BA spacer may facilitate multi-exciton Auger recombination. The 1 ns component and the long-lived component are mainly associated with trap-assisted recombination and intrinsic radiative recombination of single STEs, respectively, suggesting that iso-BAPB may introduce more trap states compared with n-BAPB.

Overall, the TA results indicate that the excited-state dynamics in both crystals are dominated by STE-related relaxation processes, including carrier cooling or STE formation, multi-exciton Auger recombination, trap-assisted recombination, and intrinsic radiative/nonradiative recombination of long-lived single STEs, as illustrated schematically in Fig. 4.7 (c,f).

Chapter 5

Conclusion and Outlook

In this thesis, the emissive-state dynamics of several quasi-2D lead halide perovskite single crystals were investigated using steady-state and time-resolved optical spectroscopy. The studied systems included n-PAPB ($n = 1$), n-PAPB ($n = 2$), n-BAPB ($n = 2$), and iso-BAPB ($n = 2$), allowing the effects of inorganic layer thickness and spacer molecular structure to be systematically compared.

Steady-state absorption and PL measurements reveal that the investigated crystals exhibit mixed quasi-2D phase characteristics dominated by low-n domains. The optical responses are strongly influenced by both the inorganic layer thickness and spacer molecular structure. Compared with n-BAPB, iso-BAPB exhibits broader and more red-shifted emission, indicating enhanced lattice distortion, stronger exciton localization, and more pronounced STE-related emission induced by the branched spacer structure.

Excitation power-dependent PL measurements indicate that the investigated excitation density region is mainly dominated by excitonic radiative recombination. Temperature-dependent PL measurements further demonstrate that both the inorganic layer thickness and spacer structure strongly influence the exciton binding energy and electron-phonon coupling behavior in quasi-2D perovskites. The extracted exciton binding energies of approximately 84-110 meV confirm the strong quantum and dielectric confinement effects in these layered structures. In particular, smaller n values lead to enhanced exciton confinement and stronger exciton localization. Meanwhile, the relatively strong electron-phonon coupling observed in the investigated crystals suggests pronounced carrier-phonon interactions and STE-related relaxation processes. Compared with the linear spacer systems, the branched iso-BA spacer induces softer lattice behavior, stronger spectral broadening, and enhanced carrier localization, indicating stronger coupling between excitons and lattice vibrations.

Femtosecond transient absorption spectroscopy further reveals that the excited-state dy-

namics in both crystals are dominated by STE-related relaxation processes. In n-BAPB, the excited carriers undergo ultrafast hot-carrier cooling and/or STE formation, followed by multi-exciton Auger recombination and long-lived intrinsic radiative/nonradiative recombination of single STEs. In iso-BAPB, the disappearance of the femtosecond component suggests ultrafast carrier cooling or STE formation within the instrumental response time. Moreover, the faster Auger recombination process indicates that the softer lattice induced by the branched iso-BA spacer facilitates multi-exciton Auger recombination. The stronger long-lived trap-related signals observed in iso-BAPB further suggest that the branched spacer structure induces more trap states and stronger carrier localization compared with n-BAPB.

Overall, this work demonstrates that both inorganic layer thickness and spacer molecular structure play critical roles in determining exciton localization, electron-phonon coupling, STE formation, and excited-state relaxation pathways in quasi-2D perovskites. Smaller n values enhance exciton confinement and localization, while branched spacer structures modify lattice dynamics, strengthen carrier-phonon interactions, accelerate STE-related relaxation processes, and increase trap-assisted recombination. These findings provide useful insight into the structure-dependent photophysics of layered perovskites and may offer guidance for tuning STE-related emission and excited-state dynamics in future perovskite light-emitting materials.

Although this work provides insight into the photophysical behavior of quasi-2D perovskite crystals, several aspects still require further investigation. First, the detailed microscopic mechanisms of STE formation and multi-exciton Auger recombination remain unclear and may require further theoretical calculations and ultrafast spectroscopy with higher temporal resolution. Second, the relationship between spacer molecular configuration, lattice softness, and trap-state formation could be further clarified through structural characterization and temperature-dependent dynamic studies. In addition, extending the investigation to a wider range of spacer molecules and n values may help establish a more comprehensive understanding of structure-property relationships in quasi-2D perovskites. Future work could focus on further understanding the microscopic mechanisms of STE formation, carrier-phonon coupling, and trap-state evolution in quasi-2D perovskites, as well as exploring their influence on future optoelectronic applications.

Bibliography

[1] Anton R Chakhmouradian and Patrick M Woodward. Celebrating 175 years of perovskite research: a tribute to roger h. mitchell. *Physics and Chemistry of Minerals*, 41(6):387–391, 2014.

[2] David B Mitzi. Synthesis, structure, and properties of organic-inorganic perovskites and related materials. *Progress in inorganic chemistry*, pages 1–121, 1999.

[3] A Von Hippel, RG Breckenridge, FG Chesley, and Laszlo Tisza. High dielectric constant ceramics. *Industrial & Engineering Chemistry*, 38(11):1097–1109, 1946.

[4] Horace Lemuel Wells. Über die cäsium-und kalium-bleihalogenide. *Zeitschrift für anorganische Chemie*, 3(1):195–210, 1893.

[5] Dieter Weber. Ch3nh3pbx3, ein pb (ii)-system mit kubischer perowskitstruktur/ch3nh3pbx3, a pb (ii)-system with cubic perovskite structure. *Zeitschrift für Naturforschung B*, 33(12):1443–1445, 1978.

[6] Maksym V Kovalenko, Loredana Protesescu, and Maryna I Bodnarchuk. Properties and potential optoelectronic applications of lead halide perovskite nanocrystals. *Science*, 358(6364):745–750, 2017.

[7] Uisik Kwon, Md Mehedi Hasan, Wenping Yin, Dasom Kim, Na Young Ha, Soonil Lee, Tae Kyu Ahn, and Hui Joon Park. Investigation into the advantages of pure perovskite film without pbi2 for high performance solar cell. *Scientific reports*, 6(1):35994, 2016.

[8] Jinsong Huang, Yuchuan Shao, and Qingfeng Dong. Organometal trihalide perovskite single crystals: a next wave of materials for 25% efficiency photovoltaics and applications beyond? *The Journal of Physical Chemistry Letters*, 6(16):3218–3227, 2015.

[9] Christian Wehrenfennig, Giles E Eperon, Michael B Johnston, Henry J Snaith, and Laura M Herz. High charge carrier mobilities and lifetimes in organolead trihalide perovskites. *Advanced Materials (Deerfield Beach, Fla.)*, 26(10):1584, 2013.

[10] EL Unger, Lukas Kegelmann, K Suchan, D Sörell, Lars Korte, and Susanne Albrecht. Roadmap and roadblocks for the band gap tunability of metal halide perovskites. *Journal of Materials Chemistry A*, 5(23):11401–11409, 2017.

[11] Quyet Van Le, Ho Won Jang, and Soo Young Kim. Recent advances toward high-efficiency halide perovskite light-emitting diodes: review and perspective. *Small Methods*, 2(10):1700419, 2018.

[12] Jiyoung Moon, Yash Mehta, Kenan Gundogdu, Franky So, and Qing Gu. Metal-halide perovskite lasers: Cavity formation and emission characteristics. *Advanced Materials*, 36(20):2211284, 2024.

[13] Daniele Cortecchia, Jun Yin, Annamaria Petrozza, and Cesare Soci. White light emission in low-dimensional perovskites. *Journal of Materials Chemistry C*, 7(17):4956–4969, 2019.

[14] Nam Joong Jeon, Jun Hong Noh, Woon Seok Yang, Young Chan Kim, Seungchan Ryu, Jangwon Seo, and Sang Il Seok. Compositional engineering of perovskite materials for high-performance solar cells. *Nature*, 517(7535):476–480, 2015.

[15] Kevin A Bush, Kyle Frohna, Rohit Prasanna, Rachel E Beal, Tomas Leijtens, Simon A Swifter, and Michael D McGehee. Compositional engineering for efficient wide band gap perovskites with improved stability to photoinduced phase segregation. *ACS Energy Letters*, 3(2):428–435, 2018.

[16] Fiona McGrath, Uma V Ghorpade, and Kevin M Ryan. Synthesis and dimensional control of cspbbr3 perovskite nanocrystals using phosphorous based ligands. *The Journal of chemical physics*, 152(17), 2020.

[17] Fei Wang, Xiang Zhang, Jinfeng Zeng, Xi Wang, Xueping Liu, Kang Zhou, Hao Wang, Chunming Yang, Haoran Lin, Yumeng Shi, et al. Dimensional control of low-dimensional perovskite hybrids for photovoltaics. *Nature Communications*, 2026.

[18] Zewen Xiao, Zhaoning Song, and Yanfa Yan. From lead halide perovskites to lead-free metal halide perovskites and perovskite derivatives. *Advanced Materials*, 31(47):1803792, 2019.

[19] Cheng-Hsin Lu, Gill V Biesold-McGee, Yijiang Liu, Zhitao Kang, and Zhiqun Lin. Doping and ion substitution in colloidal metal halide perovskite nanocrystals. *Chemical Society Reviews*, 49(14):4953–5007, 2020.

[20] Dong Yang, Ruixia Yang, Shashank Priya, and Shengzhong Liu. Recent advances in flexible perovskite solar cells: fabrication and applications. *Angewandte Chemie International Edition*, 58(14):4466–4483, 2019.

[21] Michal Baranowski and Paulina Plochocka. Excitons in metal-halide perovskites. *Advanced Energy Materials*, 10(26):1903659, 2020.

[22] Dejian Yu, Fei Cao, Chenliang Su, and Guichuan Xing. Exploring, identifying, and removing the efficiency-limiting factor of mixed-dimensional 2d/3d perovskite solar cells. *Accounts of Chemical Research*, 56(8):959–970, 2023.

[23] Fei Zhang, Dong Hoe Kim, and Kai Zhu. 3d/2d multidimensional perovskites: Balance of high performance and stability for perovskite solar cells. *Current opinion in electrochemistry*, 11:105–113, 2018.

[24] Xiaoming Zhao, Tianran Liu, and Yueh-Lin Loo. Advancing 2d perovskites for efficient and stable solar cells: challenges and opportunities. *advanced materials*, 34(3):2105849, 2022.

[25] Tik Lun Leung, Ishaq Ahmad, Ali Ashger Syed, Alan Man Ching Ng, Jasminka Popović, and Aleksandra B Djurišić. Stability of 2d and quasi-2d perovskite materials and devices. *Communications materials*, 3(1):63, 2022.

[26] Yiting Zheng, Tingting Niu, Xueqin Ran, Jian Qiu, Bixin Li, Yingdong Xia, Yonghua Chen, and Wei Huang. Unique characteristics of 2d ruddlesden–popper (2drp) perovskite for future photovoltaic application. *Journal of Materials Chemistry A*, 7(23):13860–13872, 2019.

[27] Kang Wang, Jee Yung Park, Akriti, and Letian Dou. Two-dimensional halide perovskite quantum-well emitters: A critical review. *EcoMat*, 3(3):e12104, 2021.

[28] Lei Zhang, Mingze Xia, Yuan Zhang, Li Song, Xiwei Guo, Yong Zhang, Yulei Wang, and Yuanqin Xia. The effect of organic spacer cations with different chain lengths on quasi-two-dimensional perovskite properties. *Inorganics*, 12(1):12, 2023.

[29] Xing Liu, Hejin Yan, Zheng Shu, Xiangyue Cui, and Yongqing Cai. Theoretical insights into spacer molecule design to tune stability, dielectric, and exciton properties in 2d perovskites. *Nanoscale*, 17(5):2658–2667, 2025.

[30] Diego Guedes-Sobrinho, Danilo Neves Silveira, Luis O de Araujo, Jônatas Favotto Dalmedico, W Wenzel, Y Pramudya, Maurício J Piotrowski, and Celso RC Rêgo. Revealing the impact of organic spacers and cavity cations on quasi-2d perovskites via computational simulations. *Scientific Reports*, 13(1):4446, 2023.

[31] Ning Zhou and Huanping Zhou. Spacer organic cation engineering for quasi-2d metal halide perovskites and the optoelectronic application. *Small Structures*, 3(7):2100232, 2022.

[32] Weifei Fu, Hongbin Liu, Xueliang Shi, Lijian Zuo, Xiaosong Li, and Alex K-Y Jen. Tailoring the functionality of organic spacer cations for efficient and stable quasi-2d perovskite solar cells. *Advanced Functional Materials*, 29(25):1900221, 2019.

[33] Yusheng Lei, Yimu Chen, and Sheng Xu. Single-crystal halide perovskites: opportunities and challenges. *Matter*, 4(7):2266–2308, 2021.

[34] Nadarajah Kannan and Divagar Vakeesan. Solar energy for future world:-a review. *Renewable and sustainable energy reviews*, 62:1092–1105, 2016.

[35] Rui Wang, Muhammad Mujahid, Yu Duan, Zhao-Kui Wang, Jingjing Xue, and Yang Yang. A review of perovskites solar cell stability. *Advanced Functional Materials*, 29(47):1808843, 2019.

[36] Akihiro Kojima, Kenjiro Teshima, Yasuo Shirai, and Tsutomu Miyasaka. Organometal halide perovskites as visible-light sensitizers for photovoltaic cells. *Journal of the american chemical society*, 131(17):6050–6051, 2009.

[37] Jason J Yoo, Gabkyung Seo, Matthew R Chua, Tae Gwan Park, Yongli Lu, Fabian Rotermund, Young-Ki Kim, Chan Su Moon, Nam Joong Jeon, Juan-Pablo Correa-Baena, et al. Efficient perovskite solar cells via improved carrier management. *Nature*, 590(7847):587–593, 2021.

[38] Shibo Wang, Wenhao Li, Cao Yu, Wei Shi, Qian Kang, Fengxian Cao, Kun Gao, Liu Yang, Bowen Yang, Jian Zhou, et al. Flexible perovskite/silicon tandem solar cells with 33.6% efficiency. *Nature*, 649(8095):59–64, 2026.

[39] Chuantian Zuo, Henk J Bolink, Hongwei Han, Jinsong Huang, David Cahen, and Liming Ding. Advances in perovskite solar cells. *Advanced Science*, 3(7):1500324, 2016.

[40] Abniel Machín and Francisco Márquez. Advancements in photovoltaic cell materials: silicon, organic, and perovskite solar cells. *Materials*, 17(5):1165, 2024.

[41] Lingling Mao, Constantinos C Stoumpos, and Mercouri G Kanatzidis. Two-dimensional hybrid halide perovskites: principles and promises. *Journal of the American Chemical Society*, 141(3):1171–1190, 2018.

[42] Ian C Smith, Eric T Hoke, Diego Solis-Ibarra, Michael D McGehee, and Hemamala I Karunadasa. A layered hybrid perovskite solar-cell absorber with enhanced moisture stability. *Angewandte Chemie International Edition*, 53(42):11232–11235, 2014.

[43] Zhi-Kuang Tan, Reza Saberi Moghaddam, May Ling Lai, Pablo Docampo, Ruben Higler, Felix Deschler, Michael Price, Aditya Sadhanala, Luis M Pazos, Dan Credg-

ington, et al. Bright light-emitting diodes based on organometal halide perovskite. *Nature nanotechnology*, 9(9):687–692, 2014.

[44] Sjoerd A Veldhuis, Pablo P Boix, Natalia Yantara, Mingjie Li, Tze Chien Sum, Nripan Mathews, and Subodh G Mhaisalkar. Perovskite materials for light-emitting diodes and lasers. *Advanced materials*, 28(32):6804–6834, 2016.

[45] Wenhao Bai, Tongtong Xuan, Haiyan Zhao, Haorui Dong, Xinru Cheng, Le Wang, and Rong-Jun Xie. Perovskite light-emitting diodes with an external quantum efficiency exceeding 30%. *Advanced Materials*, 35(39):2302283, 2023.

[46] Loredana Protesescu, Sergii Yakunin, Maryna I Bodnarchuk, Franziska Krieg, Riccarda Caputo, Christopher H Hendon, Ruo Xi Yang, Aron Walsh, and Maksym V Kovalenko. Nanocrystals of cesium lead halide perovskites (cspbx3, x= cl, br, and i): novel optoelectronic materials showing bright emission with wide color gamut. *Nano letters*, 15(6):3692–3696, 2015.

[47] Azhar Fakharuddin, Mahesh K. Gangishetty, Mojtaba Abdi-Jalebi, Sang-Hyun Chin, Abd. Rashid bin Mohd Yusoff, Daniel N. Congreve, Wolfgang Tress, Felix Deschler, Maria Vasilopoulou, and Henk J. Bolink. Perovskite light-emitting diodes. *Nature Electronics*, 5(4):203–216, April 2022.

[48] Yu Cao, Nana Wang, He Tian, Jingshu Guo, Yingqiang Wei, Hong Chen, Yanfeng Miao, Wei Zou, Kang Pan, Yarong He, Hui Cao, You Ke, Mengmeng Xu, Ying Wang, Ming Yang, Kai Du, Zewu Fu, Decheng Kong, Daoxin Dai, Yizheng Jin, Gongqiang Li, Hai Li, Qiming Peng, Jianpu Wang, and Wei Huang. Perovskite light-emitting diodes based on spontaneously formed submicrometre-scale structures. *Nature*, 562(7726):249–253, October 2018.

[49] Te Hu, Matthew D Smith, Emma R Dohner, Meng-Ju Sher, Xiaoxi Wu, M Tuan Trinh, Alan Fisher, Jeff Corbett, X-Y Zhu, Hemamala I Karunadasa, et al. Mechanism for broadband white-light emission from two-dimensional (110) hybrid perovskites. *The journal of physical chemistry letters*, 7(12):2258–2263, 2016.

[50] Teruya Ishihara. Optical properties of pbi-based perovskite structures. *Journal of Luminescence*, 60-61:269–274, April 1994.

[51] J.-C. Blancon, A. V. Stier, H. Tsai, W. Nie, C. C. Stoumpos, B. Traoré, L. Pedesseau, M. Kepenekian, F. Katsutani, G. T. Noe, J. Kono, S. Tretiak, S. A. Crooker, C. Katan, M. G. Kanatzidis, J. J. Crochet, J. Even, and A. D. Mohite. Scaling law for excitons in 2d perovskite quantum wells. *Nature Communications*, 9(1), 2018.

[52] Matthew D. Smith, Bridget A. Connor, and Hemamala I. Karunadasa. Tuning the luminescence of layered halide perovskites. *Chemical Reviews*, 119(5):3104–3139, January 2019.

[53] Shuangyong Sun, Teddy Salim, Nripan Mathews, Martial Duchamp, Chris Boothroyd, Guichuan Xing, Tze Chien Sum, and Yeng Ming Lam. The origin of high efficiency in low-temperature solution-processable bilayer organometal halide hybrid solar cells. *Energy Environ. Sci.*, 7(1):399–407, 2014.

[54] Kewei Wu, Ashok Bera, Chun Ma, Yuanmin Du, Yang Yang, Liang Li, and Tom Wu. Temperature-dependent excitonic photoluminescence of hybrid organometal halide perovskite films. *Phys. Chem. Chem. Phys.*, 16(41):22476–22481, 2014.

[55] Tom J. Savenije, Carlito S. Ponseca, Lucas Kunneman, Mohamed Abdellah, Kaibo Zheng, Yuxi Tian, Qiushi Zhu, Sophie E. Canton, Ivan G. Scheblykin, Tonu Pullerits, Arkady Yartsev, and Villy Sundström. Thermally activated exciton dissociation and recombination control the carrier dynamics in organometal halide perovskite. *The Journal of Physical Chemistry Letters*, 5(13):2189–2194, 2014.

[56] Kaibo Zheng, Qiushi Zhu, Mohamed Abdellah, Maria E. Messing, Wei Zhang, Alexander Generalov, Yuran Niu, Lynn Ribaud, Sophie E. Canton, and Tõnu Pullerits. Exciton binding energy and the nature of emissive states in organometal halide perovskites. *The Journal of Physical Chemistry Letters*, 6(15):2969–2975, 2015.

[57] Samuel D. Stranks and Henry J. Snaith. Metal-halide perovskites for photovoltaic and light-emitting devices. *Nature Nanotechnology*, 10(5):391–402, May 2015.

[58] Mingli Liang, Weihua Lin, Qian Zhao, Xianshao Zou, Zhenyun Lan, Jie Meng, Qi Shi, Ivano E. Castelli, Sophie E. Canton, Tönu Pullerits, and Kaibo Zheng. Free carriers versus self-trapped excitons at different facets of ruddlesden–popper two-dimensional lead halide perovskite single crystals. *The Journal of Physical Chemistry Letters*, 12(20):4965–4971, May 2021.

[59] R. T. Williams, K. S. Song, W. L. Faust, and C. H. Leung. Off-center self-trapped excitons and creation of lattice defects in alkali halide crystals. *Physical Review B*, 33(10):7232–7240, May 1986.

[60] Matthew D. Smith and Hemamala I. Karunadasa. White-light emission from layered halide perovskites. *Accounts of Chemical Research*, 51(3):619–627, February 2018.

[61] Luciana C. Schmidt, Antonio Pertegás, Soranyel González-Carrero, Olga Malinkiewicz, Said Agouram, Guillermo Mínguez Espallargas, Henk J. Bolink, Raquel E. Galian, and Julia Pérez-Prieto. Nontemplate synthesis of

ch₃nh₃pbbr₃ perovskite nanoparticles. *Journal of the American Chemical Society*, 136(3):850–853, January 2014.

[62] Michael B. Johnston and Laura M. Herz. Hybrid perovskites for photovoltaics: Charge-carrier recombination, diffusion, and radiative efficiencies. *Accounts of Chemical Research*, 49(1):146–154, December 2015.

[63] X.-Y. Zhu and V. Podzorov. Charge carriers in hybrid organic–inorganic lead halide perovskites might be protected as large polarons. *The Journal of Physical Chemistry Letters*, 6(23):4758–4761, November 2015.

[64] Claudine Katan, Nicolas Mercier, and Jacky Even. Quantum and dielectric confinement effects in lower-dimensional hybrid perovskite semiconductors. *Chemical Reviews*, 119(5):3140–3192, January 2019.

[65] Adam D. Wright, Carla Verdi, Rebecca L. Milot, Giles E. Eperon, Miguel A. Pérez-Osorio, Henry J. Snaith, Feliciano Giustino, Michael B. Johnston, and Laura M. Herz. Electron–phonon coupling in hybrid lead halide perovskites. *Nature Communications*, 7(1), May 2016.

[66] Handong Jin, Amitrajit Mukherjee, Lata Chouhan, Julian A. Steele, Flip de Jong, Yujie Gao, Maarten B. J. Roeffaers, Johan Hofkens, and Elke Debroye. Single-particle optical study on the effect of chloride post-treatment of mapbi₃ nano/microcrystals. *Nanoscale*, 15(11):5437–5447, 2023.

[67] S. Rudin, T. L. Reinecke, and B. Segall. Temperature-dependent exciton linewidths in semiconductors. *Physical Review B*, 42(17):11218–11231, December 1990.

[68] W. Becker, H. Hickl, C. Zander, K. H. Drexhage, M. Sauer, S. Siebert, and J. Wolfrum. Time-resolved detection and identification of single analyte molecules in microcapillaries by time-correlated single-photon counting (tcspc). *Review of Scientific Instruments*, 70(3):1835–1841, March 1999.

[69] Vincenzo Balzani, Paola Ceroni, and Alberto Juris. *Photochemistry and Photophysics: Concepts, Research, Applications*. Wiley-VCH, 2014.

[70] Michael Wahl. Time-correlated single photon counting. Technical note, PicoQuant GmbH, 2009.

[71] Karel Žídek, Kaibo Zheng, Carlito S. Ponseca, Maria E. Messing, L. Reine Wallenberg, Pavel Chábera, Mohamed Abdellah, Villy Sundström, and Tõnu Pullerits. Electron transfer in quantum-dot-sensitized zno nanowires: Ultrafast time-resolved absorption and terahertz study. *Journal of the American Chemical Society*, 134(29):12110–12117, 2012.

[72] Nobuaki Kitazawa Nobuaki Kitazawa. Optical absorption and photoluminescence properties of pb(i, br)-based two-dimensional layered perovskite. *Japanese Journal of Applied Physics*, 36(4R):2272, April 1997.

[73] Olga A. Lozhkina, Vyacheslav I. Yudin, Anna A. Murashkina, Vladimir V. Shilovskikh, Valentin G. Davydov, Ruslan Kevorkyants, Alexei V. Emeline, Yury V. Kapitonov, and Detlef W. Bahnemann. Low inhomogeneous broadening of excitonic resonance in mapbbr₃ single crystals. *The Journal of Physical Chemistry Letters*, 9(2):302–305, January 2018.

[74] Yang Li, Isabel Allegro, Milian Kaiser, Aditya J Malla, Bryce S Richards, Uli Lemmer, Ulrich W Paetzold, and Ian A Howard. Exciton versus free carrier emission: Implications for photoluminescence efficiency and amplified spontaneous emission thresholds in quasi-2d and 3d perovskites. *Materials Today*, 49:35–47, 2021.